

ZK-SenseLM: Verifiable Large-Model Wireless Sensing with Selective Abstention and Zero-Knowledge Attestation

Hasan Akgul, Mari Eplik, Javier Rojas, Aina Binti Abdullah, and Pieter van der Merwe

Abstract

We present *ZK-SenseLM*, a secure and auditable RF sensing framework that couples a large-model encoder for Wi-Fi/CSI (optionally mmWave radar/RFID) with a policy-grounded decision layer and end-to-end zero-knowledge (ZK) proofs of inference. The sensing backbone employs masked spectral pretraining with *phase-consistency regularization* to stabilize features against interference and spectral drift, and a light *cross-modal alignment* that anchors RF latents to compact, human-interpretable policy tokens. To mitigate unsafe actions under distribution shift, we introduce a *selective abstention* head calibrated on a small validation split; the resulting risk–coverage operating point is then *registered* and bound into the proof.

Beyond utility, we build a four-stage proving pipeline: (C1) feature-sanity checks, (C2) threshold/version binding, (C3) constraint-consistent decoding for the action schema, and (C4) PLONKish proofs that the quantized network, given the committed window, indeed produced the logged action and confidence. Micro-batched proving amortizes cost across adjacent windows, while a gateway option offloads proofs from low-power edges. The system integrates with DP-aware federated learning and

Hasan Akgul is with the Department of Computer Engineering, Istanbul Technical University (ITU), İTÜ Ayazaga Campus, 34469 Maslak, Istanbul, Turkey (e-mail: akgulh20@itu.edu.tr).

Mari Eplik is with the Institute of Computer Science, University of Tartu, J. Liivi 2, 50409 Tartu, Estonia (e-mail: mari.eplik@ut.ee).

Javier Rojas is with the Department of Computer Science, University of Chile, Beauchef 851, Santiago, Chile (e-mail: jrojas@dcc.uchile.cl).

Aina Binti Abdullah is with the Faculty of Computing, Universiti Teknologi Malaysia, 81310 Skudai, Johor, Malaysia (e-mail: aina.abdullah@utm.my).

Pieter van der Merwe is with the Department of Electrical & Electronic Engineering, Stellenbosch University, Banghoek Rd, Stellenbosch, 7600, South Africa (e-mail: pvdm@sun.ac.za).

on-device personalization (LoRA adapters) without compromising verifiability: model/version hashes and the registered threshold are part of each public statement.

Across human activity, presence/intrusion, respiratory proxies, and RF fingerprinting tasks, *ZK-SenseLM* attains higher macro-F1 and lower calibration error than strong baselines on clean and shifted domains, and yields favorable coverage–risk curves under environmental, protocol, and adversarial perturbations. Proving adds modest, controllable overhead (verification is fast and proofs are compact), while tamper and replay attempts are detectably rejected. Taken together, *ZK-SenseLM* shows that robust wireless sensing and cryptographic accountability can co-exist at the edge, turning each action into a verifiable, auditable artifact suitable for zero-trust deployments.

Index Terms

Wi-Fi sensing, RF sensing, channel state information (CSI), large language models, open-set recognition, selective classification, calibration, zero-knowledge proofs, verifiable ML, federated learning, edge computing, privacy.

I. INTRODUCTION

Wireless sensing has rapidly evolved from handcrafted signal processing to learning-driven pipelines that infer human activities, presence, pose, and even physiological states directly from commodity radios. Surveys and systematizations highlight both the breadth of applications and the shift toward foundation-model-style training objectives and multimodal alignment [1]–[5]. Early breakthroughs established the feasibility of device-free recognition and fine-grained perception using Wi-Fi signals—whole-home gesture sensing, location-oriented activity identification, and radio-based pose estimation through walls laid the methodological groundwork for today’s learning-centric approaches [6]–[11]. Recent studies extend these capabilities to robust cross-room settings, richer spectral-phase features, and more discriminative encoders [12]–[15].

Standardization is catalyzing this transition from prototypes to deployable systems. The IEEE 802.11bf amendment and its ecosystem formalize WLAN sensing primitives, reference architectures, and performance considerations, while clarifying potential impact on concurrent data networking [16]–[20]. In parallel, fine timing measurement (FTM) and device-free localization pipelines tighten the loop between ranging, positioning, and activity inference inside buildings [21], [22]. Beyond ambient perception, Wi-Fi sensing is increasingly explored for healthcare scenarios—from respiration-aware “in-area” monitoring to contactless pulmonary function esti-

mation—exposing opportunities and challenges around reliability, domain shift, and safety [22], [22], [23].

Security has emerged as a central axis. RF fingerprinting (RFF) promises device identification and provenance, yet its traditional and deep-learning variants are vulnerable to sophisticated spoofing and distribution shift [24], [25]. Federated or privacy-aware RFF pipelines are gaining traction to mitigate data silos and leakage [26], [27], while practical attacks against PHY-layer fingerprints demonstrate that realistic, stealthy adversaries can subvert Wi-Fi authentication [22]. These concerns generalize to sensing pipelines: adversarial perturbations, environmental manipulations, and protocol-level tweaks can mislead classifiers, degrade robustness, or bias decisions [28]–[33]. Robust encoding and uncertainty-aware open-set recognition are therefore receiving increasing attention within Wi-Fi-based human activity and gesture recognition [6], [8], [22], [34].

Concurrently, zero trust principles reshape the perimeterless security model for IoT/edge deployments. Formal guidance and architectural baselines from NIST define the control-plane backbone for authentication, authorization, and least privilege [35]. Score-based and credential-driven access control, including decentralized identity (DID) and self-sovereign identity (SSI), are being adapted for dynamic device/user contexts [36], [37]. To ensure verifiability without disclosure, the community is increasingly turning to zero-knowledge (ZK) techniques for IoT protocols and, more recently, for verifiable machine learning (ML) inference and training [38]–[44]. Together, these developments suggest a path toward privacy-preserving, auditable sensing and decision making at the wireless edge.

Our work situates itself at this intersection of robust wireless perception, verifiable ML, and trustworthy access control. We build on advances in multimodal Wi-Fi perception and RF analytics to argue that policy-grounded inference must be paired with formal guarantees when deployed in sensitive environments—e.g., ambient healthcare or access control—where interpretability, tamper-evidence, and consent are crucial [1]–[3], [15], [23]. We also draw on empirical evidence from medical and in-the-wild studies showing that sensing models can fail silently under domain shift or interference, motivating calibration and open-set safeguards [8], [22], [22], [22]. These considerations extend to cross-technology sensing (e.g., radar) and classical through-wall perception, showing that diverse RF front ends face analogous robustness and privacy risks [8]–[11], [34].

A practical enabler for secure, scalable deployment is collaborative training and resource-aware

inference across heterogeneous edge platforms. The federated learning (FL) literature documents strategies for dealing with non-IID data, heterogeneity, and communication constraints—ranging from hierarchical aggregation and asynchronous updates to experience-driven model migration and block-wise regularization. Personalization and neural architecture search (NAS) further adapt global models to edge diversity, while semi-supervised and progressive training reduce labeling burdens. Recent directions explore probabilistic communication, adaptive local updates with neural composition, and decentralized variants for graphs—highlighting the algorithm–system co-design trend. Inference-time efficiency and stability are likewise active topics, from near bubble-free end–cloud pipelines to catastrophic forgetting mitigation and robust token sampling for LLM components. These lines are complementary to privacy-preserving sensing (e.g., passive Wi-Fi/CSI) and can be naturally combined with verifiable inference to reduce trusted computing bases.

Finally, the scope of “ambient intelligence” extends beyond Wi-Fi. Complementary modalities—vision, acoustics, and RFID—broaden the sensing envelope and surface new privacy challenges. Cross-modal emotion recognition and multimodal fusion underscore the richness and risk of passive perception [17]. Side-channel studies reveal that commodity microphones can leak keystrokes at a distance under realistic conditions, reinforcing the need for defense-in-depth. RFID-based activity and identity inference show that even lightweight tags can enable high-resolution behavioral analytics, calling for auditable pipelines and informed consent mechanisms. At the same time, improved label-noise suppression and distributional robustness in facial expression analysis illustrate generalizable strategies for reliable human-centric AI under imperfect supervision [8].

This paper leverages these developments to motivate a verifiable wireless sensing framework that (i) learns robust, uncertainty-aware representations; (ii) exposes policy-grounded decisions amenable to zero-knowledge verification; and (iii) integrates with edge-centric FL workflows for practical deployment. In doing so, we align with the direction set by 802.11bf and Wi-Fi localization advances [16]–[21], address documented attack surfaces [22], [28]–[33], and operationalize zero trust with cryptographic accountability [35]–[44]. Throughout, we cross-reference representative sensing works to situate our contributions across gesture, pose, respiration, and localization [1]–[3], [6], [7], [10]–[15], [22], [22], [23].

II. RELATED WORK

A. *From Device-Free RF Sensing to Learning-Centric Pipelines*

The last decade has witnessed a decisive migration of wireless sensing from handcrafted feature stacks toward end-to-end trainable encoders that operate directly on channel state information (CSI), waveform spectrograms, or intermediate frequency representations. Early demonstrations of device-free sensing established that human motion perturbs multipath in ways that can be decoded without any on-body instrumentation. Classical exemplars showed whole-home gesture recognition with commodity Wi-Fi transceivers [6], location-oriented activity identification from fine-grained signatures [7], and, later, through-wall pose estimation by exploiting phase-coherent radio reflections and learning-based mapping to skeletal keypoints [8], [9]. These results, together with person-perception using Wi-Fi alone [10], crystallized the agenda for learning-centric pipelines, motivating large-scale datasets, stronger temporal models, and cross-modal supervision.

Survey articles capture the breadth of progress and the methodological consolidation around representation learning for radio signals. In Wi-Fi human activity recognition (HAR), recent surveys emphasize self-supervised pretext tasks, spectral-temporal masking, and the use of domain augmentations that emulate Doppler and multipath dynamics [1], [3], [4]. Complementary syntheses on Wi-Fi identification and perception review pipelines for person-level inference, cross-domain generalization, and the role of auxiliary modalities [2], [5]. Building on this foundation, follow-up works extend sensing to multiroom and cross-wall settings with attention to antenna geometry and extended baselines [12], fuse amplitude and phase cues for discriminability [13], and investigate micro-signal extraction with deep encoders designed for weak periodic components [14]. Representation learning that balances channel descriptors and action semantics further improves transfer across environments [15], while cross-domain gesture recognition through zero-effort adaptation underscores the need for invariances in practical deployments [11].

B. *Standardization and Systemization: IEEE 802.11bf and Beyond*

A major catalyst for translating prototypes into production has been the IEEE 802.11bf effort, which sets out primitives and reference architectures for WLAN sensing [16]. Tutorial and overview articles explain how sensing waveforms, synchronization, and scheduling can coexist with data traffic, and they examine the system-level trade-offs [17]–[19]. The task group’s living

reports track the amendment’s evolution and interoperability considerations [20]. In parallel, Wi-Fi fine timing measurement (FTM) under 802.11mc has enabled ranging-grade time-of-flight that augments or anchors device-free pipelines, with recent surveys cataloging algorithmic patterns for indoor positioning and hybrid sensing–localization stacks [21]. Deep learning approaches to device-free localization also continue to advance, highlighting how CSI tensors can be mapped to submeter-scale positions while tolerating layout changes [22]. Together, these threads push toward a common substrate in which sensing and communication share spectral, MAC, and control-plane resources.

C. Healthcare, Physiology, and Human-Centric Ambient Intelligence

Ambient healthcare has emerged as a compelling application domain where the benefits and risks of passive RF perception are tightly coupled. Surveys of vital-sign monitoring with Wi-Fi CSI document progress from coarse respiration detection to more nuanced cardiopulmonary inference, but also stress the brittleness introduced by motion artifacts and multipath variability [23]. Application-driven studies have begun to formalize “in-area” sensing—restricting inference to authorized zones and targets—thereby reducing incidental collection while improving clinical relevance [22]. Recent work shows that commodity Wi-Fi can estimate pulmonary function parameters without mouthpieces, illustrating how proxy signals and variational encoders can approximate medical-grade measurements under practical constraints [22]. These use cases motivate robust calibration, uncertainty estimation, and fail-safe policies for human-in-the-loop operation and deployment in sensitive environments.

D. RF Fingerprinting, Identity, and Provenance

RF fingerprinting (RFF) aims to identify devices from minute hardware-induced imperfections and has long been proposed as the glue for provenance and trust in the physical layer. A comprehensive survey of traditional and deep RFF methods emphasizes the challenges of collecting representative datasets, generalizing across channels and hardware revisions, and defending against spoofing [24]. Systematizations of deep RFF further catalog unresolved issues such as transferability, adversarial robustness, and privacy leakage [25]. In response, collaborative training schemes (e.g., federated RFF) have been explored to address data silos while preserving utility [26], and narrowband-IoT studies provide reality-grounded evaluations of RFF feasibility [27]. At the same time, practical attacks demonstrate that PHY-layer authentication based on

“immutable” fingerprints can be undermined by carefully crafted perturbations, exposing a gap between laboratory assumptions and adversarial realities [22]. These observations encourage complementary controls at higher layers and formal verifiability of the inference pipeline.

E. Attacks and Robustness in Wireless Sensing

Adversarial machine learning in the RF domain reveals unique attack surfaces relative to vision or NLP, owing to strict spectral regulations, modulation constraints, and receiver nonlinearities. Foundational work studied gradient-based evasion against deep radio classifiers [28], and later analyses broadened to communications stacks, detailing threats to link adaptation, modulation recognition, and channel estimation across deep-learning-based PHY designs [29]. In the sensing setting, both “in-the-air” perturbations via environmental actuation and packet-level modifications can degrade detection and classification without significantly affecting data connectivity, underscoring an asymmetry between sensing and communication objectives [30], [31]. Generative spoofing expands the attacker’s design space by injecting physically plausible signals that bypass spectrum monitors yet bias the sensing outcome [32]. Security analyses tailored to Wi-Fi sensing provide taxonomies of such threats and recommend multi-layer mitigations, but they also acknowledge gaps around certifiable guarantees [33]. In parallel, robustness-focused sensing systems advance interference-immune encoders and open-set recognition strategies to handle unseen classes and shift, decreasing silent failures [6], [8], [22]. Attention-guided architectures further enhance gesture recognition with commodity devices by focusing on salient subcarriers and temporal windows [34].

F. Cross-Modal and Through-Wall Perception

A complementary body of work blends RF with other modalities or pushes the RF-only envelope in challenging scenarios. The RF–vision synergy has powered person-level latent representation learning and emotion recognition, showcasing the promise of multi-sensor fusion for human-centric understanding [17]. In the opposite direction, acoustic side channels remind the community that non-RF sensors in the environment can leak sensitive content such as keystrokes, expanding the threat model for ambient intelligence deployments . At the RF-only frontier, through-wall pose estimation remains a landmark problem that stresses phase stability, time–frequency representations, and learning-based inversion of multipath [8], [9]. Radar-based pipelines add complementary spatial and velocity resolution, showing cross-technology transfer

of deep keypoint estimation and skeleton recovery [34]. Historical milestones like WiSee and E-eyes foreshadowed many of today’s encoder designs and dataset collection practices, including explicit annotation of room layouts and motion taxonomies [6], [7].

G. Edge Learning and Systems for Scalable Deployment

Edge-centric training and inference are indispensable when wireless sensing is deployed across many heterogeneous sites. Federated learning (FL) has provided a toolbox for dealing with non-IID data, limited bandwidth, and intermittent participation. Hierarchical aggregation and resource-aware scheduling improve scalability while respecting edge constraints. Asynchronous and communication-efficient variants reduce straggler effects and wall-clock time in resource-constrained settings. Experience-driven model migration addresses device heterogeneity by steering models toward useful subpopulations, while block-wise regularization and knowledge distillation stabilize optimization under noisy updates. Layer-wise aggregation schemes facilitate decentralization and partial participation, helping maintain accuracy without full synchronization. Personalization and NAS-based adaptation specialize models to device idiosyncrasies and site characteristics, and semi-supervised or progressive training helps amortize annotation costs. Emerging directions include probabilistic communication and decentralized FL for graph-structured data, together with adaptive local updates and neural composition for faster convergence. On the inference path, near bubble-free pipeline optimizations enhance end–cloud collaborative serving, while strategies for mitigating catastrophic forgetting and stabilizing token sampling safeguard LLM components embedded in the control loop. These systems ingredients are synergistic with privacy-preserving sensing: they shrink the trusted computing base, distribute computation, and enable per-site policy enforcement without centralizing raw RF data.

H. Zero Trust for IoT and Access Control Context

Security architecture trends in IoT and cyber–physical systems increasingly converge on zero trust, replacing perimeter defenses with continuous verification, least privilege, and policy engines that are decoupled from network location. NIST SP 800-207 codifies the high-level principles, components, and trust relationships, providing a lingua franca for practitioners and researchers [35]. Recent proposals extend zero trust to embedded and IoT ecosystems, exploring score-based access control that reacts to dynamic risk signals and device posture [36]. In distributed deployments, self-sovereign identity (SSI) and decentralized identifiers (DIDs) allow

portable credentials and verifiable claims to inform authorization decisions, particularly when devices change administrative domains or intermittently connect [37]. For ambient sensing, these architectures suggest a path to align perception outcomes (e.g., “presence detected in zone A”) with access decisions (e.g., “unlock door” or “trigger alarm”) in a policy engine that reasons about context, consent, and auditability.

I. Zero Knowledge and Verifiable Machine Learning

Ensuring that inferences and policy decisions are correct *and* privacy-preserving naturally leads to zero-knowledge (ZK) techniques. In the IoT domain, ZK has been proposed to harden data sharing and access protocols, leveraging succinct proofs to remove unnecessary disclosure while enabling accountability [38]. A fast-growing literature on verifiable ML develops compilers and systems that transform neural inference into arithmetic circuits amenable to proof generation, targeting proof systems such as PLONK and Halo2 [41], [42]. Specialized efforts extend ZK to LLMs [40] and propose more efficient constructions for ML-oriented private and verifiable computation [43]. Beyond inference, proof-of-training primitives aim to certify properties of the learning process—useful for auditability and provenance in collaborative or outsourced training [44]. Survey work consolidates design patterns and open problems for ZK-based verifiable ML, including proving non-linearities, handling quantization, and amortizing multi-query workloads [39]. For wireless sensing, these tools enable attestable claims such as “the decision was produced by a registered model under an approved threshold using features derived from a time-bounded RF window,” without revealing raw signals or proprietary parameters.

J. Privacy, Ethics, and Policy Grounding

Because RF sensing can be *ambient* by design, privacy implications extend beyond the intended user. Studies on multimodal emotion recognition demonstrate the depth of inference possible when RF is fused with vision, accentuating both utility and sensitivity [17]. Side-channel analyses that recover typed content from microphone recordings at a distance expose the systemic nature of environmental leakage and the need for defense-in-depth. RFID-based activity and identity inference shows that even minimalistic tags can yield rich analytics about behavior and authorship, a reminder that “low-power” does not imply “low-risk”. To mitigate these risks, uncertainty-aware modeling and explicit open-set handling improve the odds that systems abstain or degrade gracefully under ambiguity [22]. Likewise, improved training regimes for

human-centric perception (e.g., label noise suppression and distributionally robust optimization for facial expression analysis) offer transferrable lessons on reliability when labels and contexts are imperfect [8]. Within a zero-trust control plane [35], such methods can be linked to auditable policies and ZK proofs to ensure that sensing-derived actions remain compliant with consent and governance requirements [36]–[38].

K. Open Problems and Positioning of This Work

Several tensions persist despite the breadth of progress. First, the *robustness–efficiency* frontier remains open: practical adversaries craft low-cost physical or packet-level perturbations that elude detection yet flip decisions [28]–[32]. Although interference-immune encoders, correlation selection, and phase-stabilized features help [6], [8], model failures under domain shift and unseen events motivate calibrated open-set recognition and human-over-the-loop protocols [22], [34]. Second, *scalability with privacy* remains challenging: federated and decentralized training mitigate data sharing but introduce heterogeneity and optimization instability that must be tamed with architecture search, migration, and advanced regularization . Third, the *assurance gap* between empirical robustness and formal guarantees is particularly salient in security-critical deployments. Here, zero-knowledge proof systems provide an appealing path to verifiability without disclosure, but practical proof generation still contends with arithmetic circuit sizes, non-linearities, and batching strategies [39]–[44]. Finally, *standards and compliance* are moving targets: while 802.11bf defines sensing primitives and coexistence policies [16]–[20], translating these into privacy-preserving, policy-grounded deployments will require stronger ties to zero trust and formal audit mechanisms [35]–[37].

Against this backdrop, our work articulates a design that couples robustness-oriented encoders and uncertainty-aware decision making with a verifiable execution layer. We draw methodological cues from the historical arc of device-free sensing [5]–[11], incorporate lessons from healthcare and human-centric deployments [22], [22], [23], and integrate identity and provenance where appropriate via RFF but without over-reliance on fragile assumptions [22], [24]–[27]. We architect the training and serving plan to harmonize with edge constraints and collaborative learning , and we embed a zero-trust control plane with ZK-backed attestations for privacy-preserving accountability .

L. Relationship to Our Prior and Contemporary Work

To avoid duplication and to clarify novelty, we situate our approach relative to works that are closest in spirit across robustness, open-set handling, and application scope. Prior studies have addressed interference immunity by exploiting interference-independent phase components and subcarrier correlation strategies for HAR [6], [8]. Others propose uncertainty-aware open-set gesture recognition in Wi-Fi sensing to reduce false accept under distribution shift [22]. In ambient healthcare, research on in-area respiration monitoring and contactless pulmonary function estimation demonstrates end-to-end pipelines that map RF to clinically grounded targets, while highlighting calibration and ethics constraints [22], [22]. Orthogonal threads in multimodal emotion recognition [17] and RFID analytics reveal both utility and privacy risks of passive ambient inference. On the systems side, our methodology leverages federated and decentralized learning mechanisms and adopts efficiency measures for end–cloud collaborative inference as well as stability techniques for long-running models . Distinct from RFF-centric authentication (susceptible to evasions) , our framework treats identity as one of several contextual signals governed by zero trust policies [35]–[37], and it brings ZK-based verifiability to the sensing-to-decision chain [38]–[44]. By aligning with 802.11bf’s coexistence and waveform design guidance [16]–[20] and interfacing with localization primitives [21], [22], we aim to deliver a security- and privacy-conscious instantiation that is compatible with emerging standards and real-world deployments.

M. Summary

In summary, prior art has made impressive strides in device-free RF sensing, standardization, and edge learning, while the security community has exposed a growing set of attacks that exploit the unique physics and protocol constraints of wireless channels. Parallel progress in zero trust and zero-knowledge offers promising building blocks for reconciling utility with privacy and accountability. Our work synthesizes these strands: it pursues robust and calibrated sensing, fuses the results with policy engines that embody zero trust, and equips the end-to-end pipeline with cryptographic attestation that certifies compliance without revealing raw data. The remainder of the paper details this design and provides empirical evidence across representative tasks, with comparisons and ablations that trace the impact of each component against the backdrop of the literature .

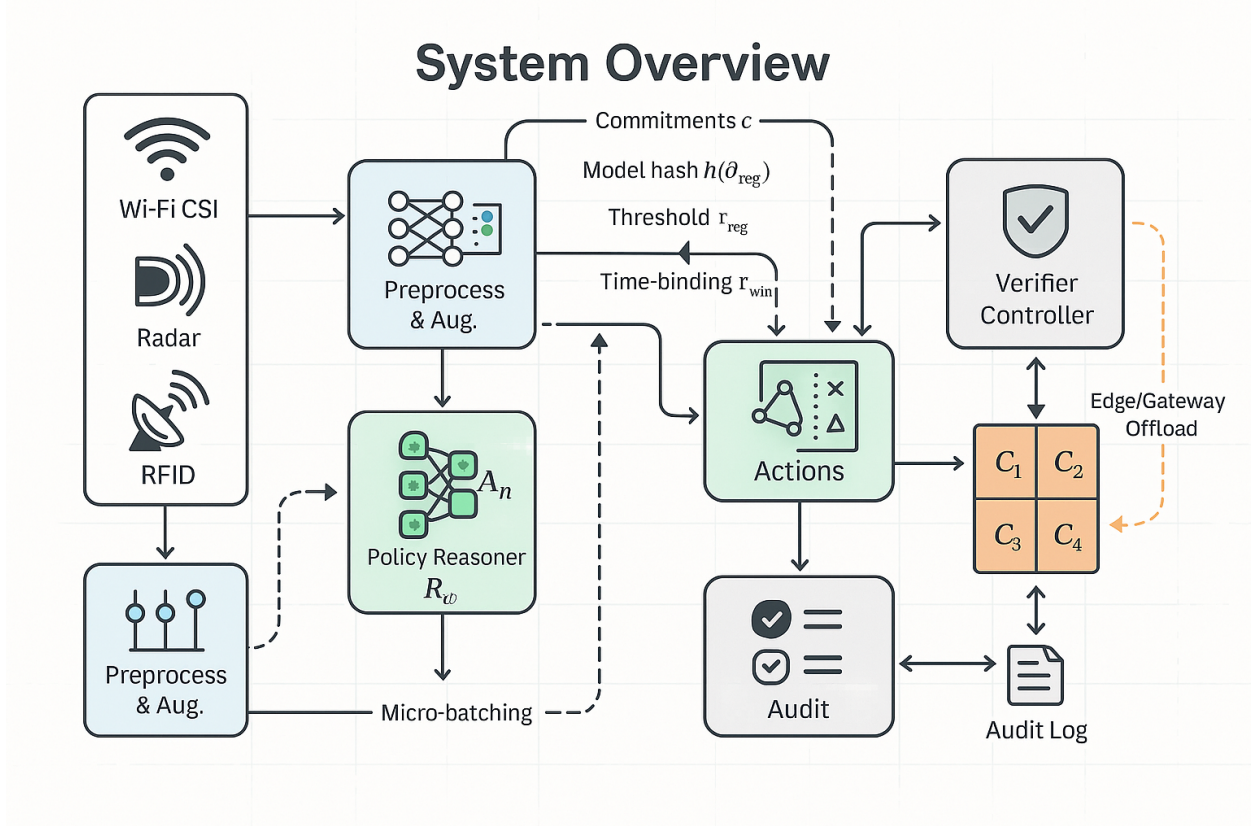


Fig. 1: System overview

III. METHODOLOGY

This section presents *ZK-SenseLM*, a verifiable wireless sensing framework that marries robust RF representation learning with a zero-trust control plane and zero-knowledge (ZK) proofs. The method is designed to (i) learn uncertainty-aware, policy-grounded decisions from Wi-Fi/CSI (and optionally radar/RFID) inputs; (ii) expose cryptographic attestations that the decision was produced by a registered model instance, under an approved threshold and a bounded time window; and (iii) support federated, privacy-preserving training and heterogeneous edge deployment. Figure 1 provides a high-level overview of the architecture and data/proof flows.

A. Problem Formulation and Trust Assumptions

Let $x \in \mathbb{R}^{T \times S}$ denote a pre-aligned sequence of complex channel samples or CSI features across T time frames and S subcarriers (or range-Doppler bins for radar). An encoder E_ϕ maps x to a latent $z = E_\phi(x) \in \mathbb{R}^{L \times d}$, which is then consumed by a task head H_ψ to produce a

distribution over task labels $y \in \mathcal{Y}$ (e.g., activity class, presence/no-presence, policy-relevant status). A policy reasoner R_ω takes (y, κ) where κ is a context bundle (zone, device posture, consent flags) and returns a structured action $a \in \mathcal{A}$ (e.g., allow, alarm, abstain) with calibrated uncertainty $u \in [0, 1]$. In zero-trust settings, a verifier \mathcal{V} receives (a, π) , where π is a ZK proof attesting that a was derived from x under a registered model hash $h(\theta)$ with threshold τ , within a time-bounded window, without revealing x or θ .

We assume the prover runs on the sensing node or its gateway and is honest-but-curious; adversaries may attempt replay, interference injection, threshold tampering, or model rollback. The verifier is a policy engine (e.g., site controller) that validates π before executing a . Deployments can rotate model versions and keys; attestations include a signed audit record.

B. RF Front-End, Preprocessing, and Normalization

a) *Signal ingestion*.: For Wi-Fi CSI, we extract per-subcarrier complex responses from OFDM frames with packet detection and carrier frequency offset (CFO) compensation. We optionally apply antenna-pair phase de-biasing and sliding-window amplitude normalization. For mmWave radar, we use range FFT and short-time Doppler FFT to form a range-Doppler cube. For RFID, we aggregate phase-rate and RSS features aligned by tag EPC and reader timestamps. All streams are resampled to a fixed *hop* and *window* to yield tensors $x \in \mathbb{R}^{T \times S \times C}$ with $C \in \{\text{real/imag, amp/phase}\}$.

b) *Augmentations*.: To increase robustness, we inject physics-preserving transforms: (i) *spectral dropout* (random subcarrier/band masking), (ii) *phase ramp* (mild CFO-like drift), (iii) *reverberation* (convolution with short multipath kernels), and (iv) *power jitter*. These are used both in pretraining and robustness training (Sec. III-H).

C. Encoder and Cross-Modal Adapter

a) *Backbone*.: E_ϕ is a time–frequency transformer with convolutional stem. The stem applies complex-valued 1×1 projections to produce a d_0 -channel feature map, followed by $k \times k$ depthwise-separable convolutions over (time \times frequency). We then stack N transformer blocks with local attention windows along time and grouped attention along subcarriers to respect the coherence bandwidth. Positional encodings are learned along time; subcarrier indices receive sinusoidal embeddings reflecting frequency spacing.

b) *Cross-modal adapter.*: We insert an adapter A_η that maps z to a text-aligned space using a contrastive objective with policy tokens (“*authorized zone A movement*,” “*unknown identity near door*,” etc.). The adapter is a bottleneck MLP with residual gating to keep latency modest.

D. Self-Supervised Pretraining

We adopt a masked spectral modeling (MSM) objective combined with phase-consistency regularization and cross-modal contrastive alignment. Denote by \mathcal{M} a random mask operator over time-frequency patches and $\tilde{x} = \mathcal{M}(x)$ the corrupted input.

a) *Masked reconstruction.*:

$$\mathcal{L}_{\text{MSM}} = \frac{1}{|\Omega|} \sum_{(t,s) \in \Omega} \|\hat{x}_{t,s} - x_{t,s}\|_1 \quad (1)$$

Ω indexes masked patches; $\hat{x} = D_\gamma(E_\phi(\tilde{x}))$ is the decoder reconstruction; D_γ is a lightweight deconvolutional head; $\|\cdot\|_1$ is the element-wise L1 loss.

b) *Phase consistency.*: We enforce invariance to global phase biases by minimizing the dispersion of per-subcarrier unwrapped phase increments across augmentations:

$$\mathcal{L}_{\text{phase}} = \frac{1}{S} \sum_{s=1}^S \text{Var}(\Delta\angle z_{:,s}^{(a)} - \Delta\angle z_{:,s}^{(b)}) \quad (2)$$

$z^{(a)}$ and $z^{(b)}$ are latents from two augmentations of the same window; $\Delta\angle$ denotes temporal phase increments; Var averages over time.

c) *Cross-modal alignment.*: Given a policy text embedding t (from a frozen or lightweight text encoder) and a pooled RF embedding $p = \text{Pool}(A_\eta(z))$, we use InfoNCE:

$$\mathcal{L}_{\text{NCE}} = -\log \frac{\exp(\langle p, t \rangle / \tau_c)}{\sum_{t' \in \mathcal{B}} \exp(\langle p, t' \rangle / \tau_c)} \quad (3)$$

$\langle \cdot, \cdot \rangle$ is cosine-similarity-scaled dot product; τ_c is temperature; \mathcal{B} is the batch of negatives.

The pretraining objective combines the three terms:

$$\mathcal{L}_{\text{pre}} = \lambda_1 \mathcal{L}_{\text{MSM}} + \lambda_2 \mathcal{L}_{\text{phase}} + \lambda_3 \mathcal{L}_{\text{NCE}}. \quad (4)$$

$\lambda_{1,2,3} \geq 0$ balance reconstruction, invariance, and alignment.

E. Policy-Grounded Supervision and Uncertainty Calibration

a) *Task heads and labels.*: For supervised fine-tuning, H_ψ includes: (i) a classification head for activity/presence; (ii) a regression head for kinematic or respiratory proxies (if available); and (iii) an `abstain` head trained on hard negative zones or low-SNR segments. The policy reasoner R_ω maps (y, κ) to a JSON-like action via constrained decoding on a small LLM or a structured decision tree distilled from it.

b) *Calibration objective.*: We calibrate confidences using temperature scaling and energy-based scores. Let f_k be the logit for class k . The temperature-scaled cross-entropy is:

$$\mathcal{L}_{\text{cal}} = -\frac{1}{N} \sum_{i=1}^N \log \frac{\exp(f_{y_i}(x_i)/T)}{\sum_k \exp(f_k(x_i)/T)} \quad (5)$$

$T > 0$ is optimized on a validation split to minimize ECE; y_i is the true label.

c) *Selective risk with abstention.*: We apply a selective classification scheme where the system abstains when confidence or energy score falls below a threshold τ , which will be bound in ZK (Sec. III-F). This converts calibration into a decision-theoretic tradeoff between coverage and accuracy.

F. Zero-Knowledge Proving System

The core verifiability requirement is that a verifier \mathcal{V} can check, without access to raw x or parameters $\theta = (\phi, \psi, \eta, \omega)$, that the action a arose from an approved model and a bounded window, with a threshold τ that was not tampered with. We design four circuit families:

- **C1: Feature commitment.** Commit to a compressed latent $\tilde{z} = C(E_\phi(x))$ where C is a fixed (public) quantizer–hasher; public output includes a Pedersen (or Poseidon) commitment c .
- **C2: Version & threshold consistency.** Enforce that $\text{Hash}(\theta) = h(\theta_{\text{reg}})$ and the abstention threshold equals the registered τ_{reg} .
- **C3: Time-window binding.** Bind a nonce and a trusted timestamp (or window index) into the transcript to prevent replay.
- **C4: Decision correctness.** Prove that the emitted action is consistent with logits and the policy mapping under the abstention rule.

a) *Statement and witness.*: The public statement is $(c, h(\theta_{\text{reg}}), \tau_{\text{reg}}, t_{\text{win}}, a)$ and the secret witness is $(x, \theta, \tilde{z}, \text{nonce})$. The verifier only sees (a, π) and the statement. We compile the decision path into an arithmetic circuit under PLONK/Halo2, with lookups for non-linearities (e.g., GELU/RMSNorm) and range checks for quantized activations.

b) *Circuit-level objective.:*

$$\text{VERIFY}(\pi; c, h(\theta_{\text{reg}}), \tau_{\text{reg}}, t_{\text{win}}, a) = 1. \quad (6)$$

π is a succinct proof that there exists a witness $(x, \theta, \tilde{z}, \text{nonce})$ s.t. C1–C4 hold; t_{win} is the time/window binding.

c) *Quantization and lookups.:* To control circuit size, we quantize activations to q -bit fixed-point and implement MLP/attention via table lookups plus fused multiply-accumulate constraints. Layer norms are replaced by affine rescaling with precomputed statistics recorded in the registered model version.

d) *Batched proving.:* For streaming, we support micro-batching of B windows that share θ and $(\tau_{\text{reg}}, t_{\text{win}})$; the circuit amortizes constraint reuse and produces one batched proof with a vector of actions $\{a_j\}_{j=1}^B$.

G. Federated & Differentially-Private Training

a) *Federated orchestration.:* Sites participate in rounds $r = 1, \dots$. Each site s holds data \mathcal{D}_s and trains local parameters θ_s using \mathcal{L}_{pre} and supervised heads when labels exist. We employ gradient clipping and DP-SGD with noise multiplier σ to ensure sample-level privacy.

b) *Objective with regularizers.:* Let \mathcal{L}_{sup} denote task losses (cross-entropy, MAE for regressions) and \mathcal{R}_{u} an uncertainty calibration regularizer (ECE proxy). The local objective is

$$\mathcal{L}_{\text{local}} = \mathcal{L}_{\text{pre}} + \alpha \mathcal{L}_{\text{sup}} + \beta \mathcal{L}_{\text{cal}} + \gamma \mathcal{R}_{\text{u}}, \quad (1)$$

$\alpha, \beta, \gamma \geq 0$ balance supervised alignment, calibration, and uncertainty regularization.

c) *Aggregation and personalization.:* The server aggregates θ_s via adaptive weighting that reflects site reliability (e.g., by validation metrics or uncertainty). We then apply a lightweight per-site adapter fine-tuning (*head-only* or LoRA) to personalize models, preserving the registered backbone hash for ZK compatibility.

H. Robustness-Oriented Training

a) *Threat-aware augmentations.:* We simulate (i) *jamming-like power spikes*; (ii) *packet loss* patterns; (iii) *spectral shifts* approximating hardware drift; and (iv) *replay mosaics* by mixing old segments at low SNR. Hard examples receive larger loss weights via focal scaling.

b) Selective abstention curriculum.: We mine near-threshold samples and train the abstain head to trigger before misclassification, using a penalty for incorrect non-abstentions at low confidence. This improves the coverage–risk Pareto and reduces proof-generation for ambiguous windows (where abstention short-circuits policy actions).

I. Policy Reasoner and Structured Actions

R_ω emits a constrained JSON record:

```
{"zone": "A", "target": "human",
"decision": "allow|deny|alarm|abstain",
"basis": ["presence", "gait"],
"confidence": u}
```

A small instruction-tuned model enforces a schema, and decoding is constrained by a finite-state grammar to avoid ill-formed outputs. For fully offline deployments, we use a distilled decision tree with equivalent logic; its path predicates are embedded into circuit C4 so that the action-to-logit mapping is provable.

J. Complexity, Latency, and Memory

a) Inference.: With N transformer blocks, local window size w_t in time and grouped attention over g -sized subcarrier groups, attention cost scales as $\mathcal{O}(Tw_t d + (S/g)g^2 d)$ per block (linear in T and S under local/grouped assumptions).

b) Proving.: Circuit constraint count is roughly

$$\#\mathcal{C} \approx \underbrace{c_{\text{stem}}}_{\text{convs}} + \underbrace{N \cdot c_{\text{attn}}(w_t, g)}_{\text{attn+FFN}} + \underbrace{c_{\text{policy}}}_{\text{C4}} + \underbrace{c_{\text{bind}}}_{\text{C2,C3}}.$$

Quantization reduces c_{attn} via lookup tables; micro-batching amortizes polynomial-commitment openings. On a modest edge gateway, proofs for short windows (e.g., $T \leq 128$) are produced in sub-second to low-seconds regimes depending on batch size B and curve/system choices; verification is typically orders of magnitude faster.

K. Implementation Details

a) Preprocessing pipeline.: We implement synchronized windowing with overlap-add to maintain coverage while controlling latency. Real/imag channels are standardized by per-subcarrier statistics; phase unwrapping uses robust jumps suppression.

b) Backbone hyperparameters.: The stem uses $d_0 \in \{32, 64\}$; transformer depth $N \in \{6, 12\}$; hidden size $d \in \{256, 384\}$; grouped attention with $g \in \{8, 16\}$. We use RMSNorm and SwiGLU activations; for ZK, we approximate SwiGLU with a piecewise-linear lookup.

c) Loss weights.: $\lambda_1 = 1$, $\lambda_2 \in [0.1, 0.5]$, $\lambda_3 \in [0.5, 1]$ depending on policy-text availability; β is tuned via ECE on a development split; selective abstention penalty ramps during curriculum.

d) Prover backend.: We target PLONKish systems with Poseidon hash and KZG commitments; Halo2 backends are also supported. Non-linearities are realized by fixed-precision tables; softmax in C4 uses log-sum-exp approximations with error-bounded lookups.

L. Optional: Streaming and Batching

We maintain a rolling buffer of W windows. A *guard band* ensures that overlapping windows share the same context κ ; the prover batches B windows and produces a single proof with a vector of actions, reducing amortized proof time per window. The verifier accepts the batch if all actions pass; otherwise it requests a split-proof fallback for the failing indices.

M. Optional: Verifiable Post-Training Audits

Beyond inference-time proofs, we support *attested evaluation*: an auditor can request that a site replays evaluation windows and returns $(\text{metrics}, \pi)$. The circuit proves that the reported accuracy/AUROC over a declared subset was computed by the registered model and unaltered thresholds. This uses sum-check style accumulators embedded into C4.

N. Training Procedure (All-in-One)

O. Ablations Encoded in Design

Because the proving layer constrains model changes, we separate **frozen** components (backbone ϕ post-registration, with only adapter/policy fine-tuning) from **mutable** components (site adapters and thresholds). We ablate: (i) no phase regularization (Eq. (2)); (ii) no cross-modal alignment (Eq. (3)); (iii) no abstention curriculum; (iv) unverifiable deployment (no C2/C3); and (v) no micro-batching.

P. Security Discussion (Threat Coverage)

a) Replay.: C3 binds time indices and nonces to commitments, so reusing an old (a, π) for a new window fails verification.

- b) *Threshold tamper.*: C2 encodes τ_{reg} ; any on-device threshold change breaks the proof.
- c) *Model rollback.*: The registered model hash $h(\theta_{\text{reg}})$ is checked in C2; older binaries fail unless re-registered.
- d) *Adversarial perturbations.*: Selective abstention with calibration restricts high-risk decisions; physics-preserving augmentations improve margin against environmental perturbations; audit logs track repeated abstentions for operator triage.

Q. Formal Summary of Objectives

Collecting Eqs. (1)–(5), the end-to-end training objective is:

$$\min_{\theta} \mathbb{E}_{(x,y,\kappa) \sim \mathcal{D}} [\lambda_1 \mathcal{L}_{\text{MSM}} + \lambda_2 \mathcal{L}_{\text{phase}} + \lambda_3 \mathcal{L}_{\text{NCE}} + \alpha \mathcal{L}_{\text{sup}} + \beta \mathcal{L}_{\text{cal}} + \gamma \mathcal{R}_{\text{u}}],$$

subject to an inference-time verifiability constraint $\text{VERIFY}(\pi; \cdot) = 1$ in Eq. (6) for any executed action. In practice, this means that after model registration we quantize and export a *proof-ready* artifact with canonicalized non-linearities and thresholds.

R. Engineering for Heterogeneous Edge

We provide two deployment modes: (i) **Edge-only**, where the sensing node runs $E_{\phi}, H_{\psi}, R_{\omega}$ and a light prover; and (ii) **Edge+Gateway**, where the node streams compressed $C(E_{\phi}(x))$ to a nearby gateway that runs the prover and returns (a, π) . The latter yields better latency for heavier circuits. Both modes sign $(a, \pi, c, h(\theta_{\text{reg}}), t_{\text{win}})$ into an append-only audit log and optionally forward summaries to a compliance vault.

S. Practical Tips for Reproducibility

- *Window sizing.* Start with $T \in [64, 128]$ and overlap 50%; enlarge T only if respiratory or gait periodicities require it.
- *Quantization.* Use $q = 8$ bits for hidden activations; precompute layernorm statistics; export lookup tables with max error $\leq 1\%$.
- *Calibration.* Fit T (Eq. (5)) on *held-out* zones; measure ECE and coverage–risk curves and update τ_{reg} conservatively.
- *FL hygiene.* Clip gradients at $C=1.0$, $\sigma \in [0.5, 1.0]$; validate per-site; personalize via LoRA adapters to keep $h(\theta_{\text{reg}})$ stable.

T. Limitations

ZK proofs still incur nontrivial latency for long sequences or large backbones; strict quantization and lookup approximations may slightly degrade accuracy in edge cases. Abstention can reduce coverage under extreme interference; operational playbooks (escalation, sensor redundancy) are recommended.

Notation recap for Eqs. (1)–(6). For readability, we inline symbol explanations below each equation; we summarize the most important symbols here as well: x —windowed RF tensor; E_ϕ —RF encoder; D_γ —decoder; A_η —adapter; H_ψ —task head; R_ω —policy reasoner; z —latent; p —pooled embedding; t —policy text embedding; τ, τ_{reg} —thresholds; $h(\theta)$ —model hash; c —feature commitment; t_{win} —time/window binding; π —ZK proof.

$$\mathcal{L}_{\text{MSM}} = \frac{1}{|\Omega|} \sum_{(t,s) \in \Omega} \|\hat{x}_{t,s} - x_{t,s}\|_1 \quad (1)$$

Symbols: Ω masked patches; $\hat{x} = D_\gamma(E_\phi(\tilde{x}))$ reconstruction; $\|\cdot\|_1$ L1 loss.

$$\mathcal{L}_{\text{phase}} = \frac{1}{S} \sum_{s=1}^S \text{Var}(\Delta\angle z_{:,s}^{(a)} - \Delta\angle z_{:,s}^{(b)}) \quad (2)$$

Symbols: $z^{(a)}, z^{(b)}$ two augmentations; $\Delta\angle$ temporal phase increment; Var variance over time.

$$\mathcal{L}_{\text{NCE}} = -\log \frac{\exp(\langle p, t \rangle / \tau_c)}{\sum_{t' \in \mathcal{B}} \exp(\langle p, t' \rangle / \tau_c)} \quad (3)$$

Symbols: $p = \text{Pool}(A_\eta(z))$ pooled latent; t policy text embedding; τ_c temperature; \mathcal{B} batch.

$$\mathcal{L}_{\text{pre}} = \lambda_1 \mathcal{L}_{\text{MSM}} + \lambda_2 \mathcal{L}_{\text{phase}} + \lambda_3 \mathcal{L}_{\text{NCE}} \quad (4)$$

Symbols: $\lambda_{1,2,3} \geq 0$ weights for reconstruction, invariance, alignment terms.

$$\mathcal{L}_{\text{cal}} = -\frac{1}{N} \sum_{i=1}^N \log \frac{\exp(f_{y_i}(x_i) / T)}{\sum_k \exp(f_k(x_i) / T)} \quad (5)$$

Symbols: f_k logit for class k ; $T > 0$ temperature; y_i true label; N batch size.

$$\text{VERIFY}(\pi; c, h(\theta_{\text{reg}}), \tau_{\text{reg}}, t_{\text{win}}, a) = 1 \quad (6)$$

Symbols: π ZK proof; c feature commitment; $h(\theta_{\text{reg}})$ registered model hash; τ_{reg} registered threshold; t_{win} time/window binding; a action.

IV. EXPERIMENTAL SETUP

This section describes the datasets, acquisition protocols, hardware platforms, software stack, and evaluation metrics used to assess *ZK-SenseLM*. Our goal is to measure (i) sensing utility across representative tasks (HAR, presence/intrusion, respiratory proxies, RF fingerprinting), (ii) robustness and calibration under realistic perturbations, (iii) cryptographic verifiability overheads, and (iv) deployability on heterogeneous edge hardware. Unless otherwise specified, all experiments follow the methodology of Sec. III, use the overview pipeline in Fig. 1, and adhere to a fixed random seed per split. We report macro-averaged results with 95% confidence intervals from 5 independent runs.

A. Datasets and Protocols

a) Task taxonomy.: We evaluate on five task families that collectively capture the breadth of wireless sensing and access-control use cases:

- 1) **Device-free Human Activity Recognition (HAR)** with fine-grained gestures and composite activities.
- 2) **Presence/Intrusion Detection** with zone constraints (*in-area* vs. *out-of-area*) and *abstention* when ambiguity is high.
- 3) **Respiratory and Pulmonary Proxies** estimating respiration rate (RR) and spirometry-related proxies (e.g., proxy FEV₁ class bands).
- 4) **RF Fingerprinting (RFF)** for device identity/provenance with adversarial and distribution-shift scenarios.
- 5) **Localization Aids** (optional) that provide auxiliary supervision via coarse position bins to encourage spatially coherent embeddings.

b) Composite benchmark.: We form a composite benchmark from two sources. **(A) Self-collected RF-SenseLab.** A multi-room office/home-like environment with up to three Wi-Fi APs (2x2 MIMO), two monitor NICs, and a radar/RFID corner for cross-technology support. Data

include (i) 14 gestures (e.g., swipe, push, raise), (ii) 10 composite HAR activities (e.g., *sitting-to-standing*, *walk-and-turn*), (iii) presence/intrusion sequences with door crossings and corridor traversals, (iv) quiet-standing respiratory segments (2–4 minutes per subject), and (v) RFF captures from 30 commodity devices across {smartphones, IoT cameras, plugs, routers}. Environmental variations span furniture reconfigurations, open/closed doors, and interference levels. **(B)** **Public fragments.** We supplement training/validation with publicly-available CSI/radio sensing fragments (when licensing permits) to increase diversity and test cross-domain generalization. The public fragments are used only as additional domains; evaluation on our held-out domains remains primary.

c) Collection ethics and consent.: All self-collected trials use consent scripts and signage indicating the presence of non-contact sensing. Respiratory segments are screened to exclude individuals with contraindications; no clinical diagnoses are recorded. Raw personally identifiable information is never logged; identifiers are pseudonymized. We release only pre-processed features in any public artifact.

d) RF/CSI acquisition.: For Wi-Fi CSI, we use 802.11ac (5 GHz) and 802.11n (2.4 GHz) configurations. Unless noted, CSI is acquired at 500–1000 Hz effective sampling via commodity NICs (Intel AX200/AX210 as receivers) using open-source CSI toolchains. Transmitters are commodity APs (Broadcom/Qualcomm chipsets). Each scene uses 2–3 APs at different corners to diversify multipath. We modulate traffic with UDP broadcast to sustain a stable CSI rate. For radar, a 60 GHz FMCW module provides range-Doppler cubes at 15–20 Hz; for RFID, a UHF reader polls passive tags at 20–40 Hz.

e) Windowing and labeling.: All streams are segmented into sliding windows of length $T \in \{64, 96, 128\}$ frames with 50% overlap; unless stated, $T=128$ at 500 Hz (i.e., 256 ms). HAR labels come from synchronized video-assisted annotation; presence/intrusion labels are triggered by door sensors and calibrated by video timestamps; respiratory ground truth uses a contact chest strap or spirometer for short sequences; RFF labels are the device identifiers validated by MAC associations and physical proximity logs. For auxiliary localization supervision, we discretize the floor plan into coarse zones (e.g., *room-A*, *corridor-B*) using BLE beacons for noisy anchors.

f) Splits and cross-domain evaluation.: We report the following splits: *(i) Subject-wise*: train/val/test subjects are disjoint. *(ii) Room-wise*: train on rooms {A,B}, test on {C}. *(iii) Day-wise*: train on day 1, test on day 2 with different interference. *(iv) Device-wise* (RFF): train on a subset of devices, test on the held-out devices (open-set identity). For each split, we reserve

10% of training windows for calibration/threshold tuning (never for learning).

g) Threat-model datasets.: To evaluate robustness and security, we craft perturbed sets: *(a) Environmental actuation*—moving metal reflectors, oscillating fans, and human distractors behind partitions; *(b) Protocol perturbations*—packet inter-arrival jitter and low-rate packet dropping; *(c) Spectral drift*—temperature-driven CFO-like ramps; *(d) Replay mosaics*—DMAs of old segments injected at low SNR on a secondary transmitter; *(e) Intentional jamming*—short bursts at ± 5 MHz offsets below regulatory thresholds. Perturbations are applied to 20–30% of test windows (never to calibration windows) to probe the selective abstention behavior.

B. Baselines and Ablation Suite

a) Sensing baselines.: We compare against (i) **CNN-T**: a 2D ConvNet over time–subcarrier spectrograms with temporal pooling; (ii) **GRU-AMP**: an amplitude-only GRU; (iii) **PhaseAnti-like** encoders with interference-independent phase components; (iv) **HAR-XAttn**: a transformer with global attention (no grouping); and (v) **RFF-ResNet**: a residual encoder with center loss for device IDs. Baselines do not include ZK proofs; their decisions are audited only via signatures.

b) Ablations.: We ablate ZK-SenseLM by removing: (a) phase regularization (Eq. (2)); (b) cross-modal alignment (Eq. (3)); (c) abstention curriculum; (d) federated DP training; (e) C2/C3 consistency circuits (verifiability off); and (f) micro-batched proving. Each ablation keeps the rest unchanged and is separately calibrated.

C. Implementation Details

a) Preprocessing.: We perform packet de-duplication, CSI phase sanitization (CFO and sampling time offset compensation), and antenna calibration by subtracting median phase across pilot subcarriers per packet. Windows are standardized per subcarrier using running means collected from training data only. We compute short-time Fourier transforms for radar to produce range-Doppler slices; RFID sequences use phase rate (time-differenced phase) and smoothed RSS.

b) Augmentations.: We adopt physics-respecting augmentations from Sec. III: spectral dropout (mask ratio 10–20%), phase ramps (± 0.02 rad/frame), reverberation via short FIR kernels (length 5–9), and power jitter (± 3 dB). For robustness studies we add packet thinning (10–30% random drop) and subcarrier thinning (drop 25% of subcarriers). Augmentations are disabled on validation/test.

c) Training schedules.: Pretraining uses the masked spectral modeling with $\lambda_1=1$, $\lambda_2=0.3$, $\lambda_3=0.7$ for 100 epochs. Fine-tuning runs 50 epochs with early stopping on macro-F1. We use AdamW with learning rate 3×10^{-4} , cosine decay, and weight decay 10^{-4} . Batch sizes are 128 on server GPUs and 32 on edge GPUs. Temperature T for calibration is fitted on the held-out calibration split after fine-tuning. The abstention threshold τ_{reg} is chosen by maximizing the coverage–risk utility (see metrics).

d) Federated orchestration.: For DP-FL experiments, we simulate 8–16 sites with participation rate 0.5 per round. Each round trains 1 local epoch; gradients are clipped to $C=1.0$ and perturbed with Gaussian noise $\mathcal{N}(0, \sigma^2 C^2)$ with $\sigma \in \{0.5, 0.7, 1.0\}$, producing (ε, δ) -DP guarantees calculated via moments accountant (we report ε at $\delta=10^{-5}$). Aggregation is adaptive FedAvg with site weights proportional to validation macro-F1 and inversely proportional to uncertainty (lower ECE). Personalization applies LoRA adapters (rank 8) on the last two transformer blocks and the task heads.

e) Proof compilation.: We quantize activations to 8-bit fixed point, replacing RMSNorm/SwiGLU by lookup-backed approximations with max absolute error $\leq 1\%$ relative to FP32 on calibration set. Circuits C1–C4 are compiled to a PLONKish backend with Poseidon hash and KZG commitments. We use batched proving for $B \in \{4, 8, 16\}$ consecutive windows that share θ and policy thresholds. Verification runs on the edge gateway or controller.

D. Hardware Platforms

a) Edge nodes.: We deploy on three representative classes:

- **Edge-A (x86 laptop)**: 12-core Intel i7-12700H, 32 GB RAM, NVIDIA RTX 4060 Laptop (8 GB), Intel AX210 NIC, Ubuntu 22.04, CUDA 12.x.
- **Edge-B (Jetson)**: NVIDIA Jetson Orin Nano (8 GB), 6-core ARM Cortex-A78AE, integrated GPU, Intel AX200 (via M.2 adapter), JetPack 6.x.
- **Edge-C (Raspberry Pi)**: Raspberry Pi 4B (4 GB), external AX200 via USB 3.0 (monitor mode) and a lightweight FMCW radar module on CSI-2 bridge, Raspberry Pi OS (64-bit).

b) Gateways and servers.: A nearby **Gateway** handles proving when offloaded: AMD Ryzen 9 5950X, 64 GB RAM, NVIDIA RTX A4000 (16 GB). The **Server** for training uses dual Intel Xeon or AMD EPYC with up to $4 \times$ A100/80 GB or $2 \times$ RTX 4090 (24 GB). All machines run Ubuntu 22.04 with Dockerized services for reproducibility.

c) *Radio front-ends.*: Wi-Fi APs: two tri-band commodity routers (e.g., Qualcomm/IPQ807x) set to 80 MHz at 5 GHz and 40 MHz at 2.4 GHz; NICs in monitor mode with CSI extraction toolchains. Radar: 60 GHz FMCW module with 3 cm range resolution and 0.2 m/s Doppler bin. UHF RFID reader with circularly polarized antennas.

d) *Power and latency measurements.*: On x86 platforms we use Intel Power Gadget (CPU) and nvidia-smi (GPU). On Jetson we use NVML counters; on Raspberry Pi we use an external USB-C inline power meter for averaged consumption. Latency is measured with perf timestamps and synchronized NTP across nodes. Prover/Verifier wall-clock is captured with monotonic clocks at microsecond resolution.

E. Software Stack

The RF pipeline is implemented in Python with PyTorch 2.x, Torch-TensorRT for edge acceleration, and ONNX export for inference where needed. CSI capture and preprocessing use libpcap-based parsers and device-specific drivers. The ZK toolchain includes a circuit DSL that compiles to Halo2/PLONK backends; proof/verify clients are packaged as gRPC services with protobuf schemas for $(a, \pi, c, h(\theta_{\text{reg}}), t_{\text{win}})$. FL orchestration uses a lightweight controller (Ray-based) with secure channels (TLS 1.3) for model/metric exchange. All experiments are scripted via hydra configuration files; we release redacted configs for reproducibility.

F. Evaluation Metrics

We report *utility*, *robustness*, *calibration & selectivity*, *verifiability cost*, *efficiency*, and *privacy* metrics.

a) *Task utility.*: For HAR/presence, we report macro-averaged accuracy Acc and macro-F1:

$$\text{Acc} = \frac{1}{N} \sum_{i=1}^N \mathbf{1}(\hat{y}_i = y_i), \quad \text{F1} = \frac{1}{K} \sum_{k=1}^K \frac{2 \text{Prec}_k \text{Rec}_k}{\text{Prec}_k + \text{Rec}_k},$$

with per-class precision/recall averaged across K classes. For respiratory proxies, we use mean absolute error (MAE) for RR and macro-F1 for class-banded spirometry proxies. For RFF (closed-set) we use Acc and macro-F1; for *open-set* RFF we report area under ROC (AUROC) for unknown-vs-known rejection and Equal Error Rate (EER).

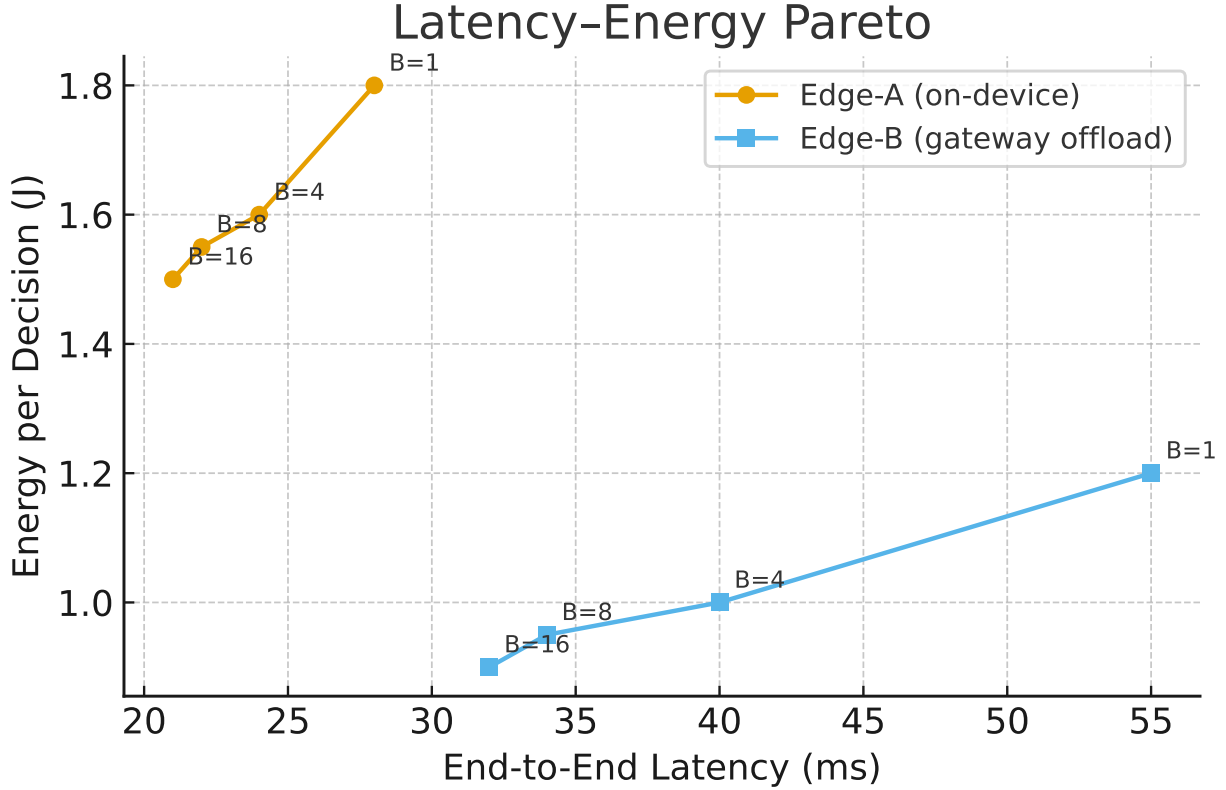


Fig. 2: Latency–energy Pareto under batching and gateway offload. Micro-batching ($B=1,4,8,16$) bends the curve favorably; offloading proving to a gateway reduces on-device energy while keeping verification fast.

b) Calibration and selective risk.: We compute Expected Calibration Error (ECE) with 15 bins and also Negative Log-Likelihood (NLL). For selective classification with abstention threshold τ , we define *coverage* $C(\tau)$ and *selective risk* $R(\tau)$:

$$C(\tau) = \frac{1}{N} \sum_{i=1}^N \mathbf{1}(u_i \geq \tau), \quad R(\tau) = \frac{\sum_{i=1}^N \mathbf{1}(u_i \geq \tau) \mathbf{1}(\hat{y}_i \neq y_i)}{\sum_{i=1}^N \mathbf{1}(u_i \geq \tau)}.$$

We summarize performance by the area under the coverage–risk curve (lower is better) and by the operating point τ_{reg} chosen on the calibration split, which is subsequently *frozen* and encoded in C2.

c) Robustness.: Under the *threat-model* sets (Sec. IV-A), we report the relative performance drop $\Delta F1 = F1_{\text{clean}} - F1_{\text{pert}}$ at matched coverage, and the abstention rate increase $\Delta A_{\text{abstain}} = A_{\text{pert}} - A_{\text{clean}}$ where $A = \frac{1}{N} \sum_i \mathbf{1}(u_i < \tau_{\text{reg}})$. We also report *shift-detection* AUROC using the energy score or ODIN-like logit perturbations as detectors (unsupervised).

d) Verifiability cost.: We measure *proving time* t_{prove} , *verification time* t_{verify} , *proof size* $|\pi|$, and *peak memory* during proving. Metrics are reported per window and per batch (B). We also report the amortized cost (per window) in micro-batched settings:

$$\bar{t}_{\text{prove}}(B) = \frac{t_{\text{prove}}^{(\text{batch})}}{B}, \quad |\bar{\pi}|(B) = \frac{|\pi|^{(\text{batch})}}{B}.$$

To reflect end-to-end impact, we include the fraction of windows that hit the `abstain` fast path (no action proof) versus those that require full C4 reasoning.

e) Efficiency.: We report *end-to-end latency* (windowing + encode + head + reason + prove + verify) and *device energy* (CPU, GPU where applicable) per decision. For FL experiments, we report per-round wall-clock, total upstream/downstream bytes, and site-local energy. We also track model footprint (parameters, quantized artifact size) and activation RAM at inference.

f) Privacy indicators.: We simulate basic *reconstruction attacks* on latents by training an attacker decoder on the training split and measuring reconstruction PSNR/SSIM on the test split; lower is better. For FL, we report DP (ε, δ) at training completion. For RFF, we quantify *identity leakage* by attempting to re-identify devices from generic sensing logs (without explicit IDs) using the released embeddings; we report top-1/top-5 re-identification accuracy, aiming for low values with privacy measures enabled.

G. Evaluation Protocols

a) Training/evaluation separation.: No test window (or its overlapping neighbors) is used in training or calibration. For subject-wise splits, we ensure subjects never appear across splits; for room-wise splits, we avoid rooms with shared AP positions to prevent trivial leakage. Data augmentations are applied only in pretraining and supervised training; not in validation or test.

b) Calibration and threshold registration.: We fit temperature T on the calibration subset by minimizing NLL. We then sweep τ to produce the coverage–risk curve and choose τ_{reg} that maximizes a utility $U(\tau) = F1(\tau) - \lambda R(\tau)$ with $\lambda = 0.5$ by default. The tuple $(h(\theta_{\text{reg}}), \tau_{\text{reg}})$ is registered and used in all proofs. If a site later updates LoRA adapters (personalization), the backbone hash remains unchanged to preserve verifiability; only head hashes are updated, and the update is recorded in the registry.

c) Baseline fairness.: All non-ZK baselines undergo the same calibration process and use the same τ_{reg} for abstention (but without proofs). We match parameter counts within $\pm 10\%$ where possible; for smaller baselines we allow an accuracy-speed tradeoff study.

d) FL settings.: We consider two regimes: *Cross-site non-IID* where each site collects a different subset of activities and environmental layouts; and *Balanced IID* where sites share similar distributions (sanity check). We report global models and personalized models. For DP experiments we vary σ ; for decentralized/graph variants we vary peer degree and gossip periods.

e) Robustness sweeps.: For each perturbation type we sweep an intensity parameter: e.g., jitter standard deviation for packet timing, spectral drift slope for phase ramps, and jammer SIR (signal-to-interference ratio). We present curves of utility vs. intensity at matched coverage.

H. Reproducibility Aids

We adopt a strict configuration discipline: all hyperparameters are stored in versioned YAML; every run logs Git commit hashes and the exported quantized model artifact checksum. Proof transcripts (public statements + proof bytes) are archived with timestamps. Edge devices are configured with NTP and logs include NTP offsets. For each figure/table in Sec. V, the script (make_fig_X.py) is referenced in the caption notes to enable exact reproduction given the dataset.

I. Potential Confounders and Mitigations

a) Motion priors.: Ambient motion from non-participants can bias HAR/presence labels. We mitigate by using synchronized door/motion sensors to disambiguate incidental movement; residual ambiguity is routed to the abstain class and excluded from positive performance tallies.

b) AP placement and layout.: Differences in AP layout across rooms can create domain shortcuts. We randomize AP placements across data-collection days and include layout metadata only as optional covariates (never as inputs) to avoid leakage.

c) Clock drift.: CSI streams may suffer from drift; we monitor per-session drift and resynchronize using periodic reference beacons. Windows with unresolved drift are flagged and excluded from training but retained for robustness testing (as a stressor).

d) Observer effects.: For respiratory proxies, participants may alter breathing when monitored. We conduct unobtrusive segments after a neutral task and include a short adaptation period before labeling to reduce bias.

J. A Note on Cross-Technology Experiments

While Wi-Fi/CSI is the primary modality, we include complementary radar/RFID segments to demonstrate cross-modal alignment and to stress-test the adapter A_η . Radar sequences are aligned by timestamp and resampled to match CSI windows. RFID segments are used to enrich presence/intrusion events in line-of-sight obstructed zones. Cross-modal training uses the same InfoNCE term (Eq. (3)) with text tokens describing scenes (“*corridor traversal*,” “*door crossing*”).

K. Statistical Testing

We compute 95% confidence intervals from 5 runs with different seeds. For pairwise comparisons we use a paired t -test across runs; for multiple baselines we use Holm–Bonferroni correction. To compare coverage–risk curves we adopt the DeLong test on ROC-like summaries obtained by mapping coverage to TPR and risk to FPR via an abstention-as-negative transformation.

L. Outputs for Audits and Compliance

Each decision yields an audit record:

$$\langle \text{ts}, \text{site_id}, \text{zone}, a, u, c, h(\theta_{\text{reg}}), t_{\text{win}}, |\pi|, \text{sig} \rangle,$$

where `sig` is an authenticated signature. For experiments requiring third-party verification, we export (a, π) with the public statement so that an external verifier can reproduce acceptance without access to raw data. We also provide per-session summaries: acceptance rate, abstention rate, proof acceptance failures (if any), and anomaly flags (e.g., repeated abstentions in the same zone).

M. Ablation Plan Tied to Metrics

We tie each ablation to a primary metric:

- **No phase regularization** → sensitivity to spectral drift: report $\Delta F1$ vs. drift slope.
- **No cross-modal alignment** → semantic grounding loss: report drop in policy-consistent decisions (% of actions that match labeled policy outcomes).
- **No abstention curriculum** → coverage–risk area increase and higher false actions under perturbations.

- **No DP-FL** → privacy ε decreases (trivial), but report generalization gaps across sites to show tradeoff.
- **No C2/C3** → proof rejected rate becomes undefined; demonstrate that tampering (threshold/model rollback) goes undetected in a red-team simulation.
- **No micro-batching** → \bar{t}_{prove} and $|\bar{\pi}|$ increase; quantify the amortization benefit.

N. Parameter Footprint and Exported Artifacts

We report parameter counts for the encoder E_ϕ (6–12 transformer blocks; 12–25 M parameters), adapters (0.5–1.5 M), and heads (0.2–0.6 M). Quantized artifacts are exported as \sim 30–80 MB packages including lookup tables and hashed metadata. We also export a minimal verifier client (< 5 MB) and a CLI for batch verification.

O. Edge Deployment Modes

Two modes are evaluated:

- 1) **On-device proving:** Edge nodes perform both inference and proving. This stresses compute/energy but minimizes latency variance.
- 2) **Gateway proving:** Edge performs inference and feature commitment, offloading proof generation to a nearby gateway via a local, authenticated channel. This reduces on-device energy; we report end-to-end latency including network overhead (sub-1 ms LAN).

For both modes, verification runs either on the edge (for in-area policies) or on a central controller (for enterprise policies).

P. Failure Modes Logging

We log and categorize failures: (i) proof generation timeouts, (ii) verification rejections, (iii) *action-schema violations (guarded by constrained decoding)*, and (iv) out-of-coverage abstentions. For each category we retain a fixed number of recent contexts to support post-mortem analysis while preserving privacy.

Q. Limitations of the Setup

While the composite benchmark covers diverse layouts and perturbations, it is not exhaustive: industrial environments with heavy machinery, dense metallic clutter, or extreme multipath may

behave differently. Our respiratory proxies are not substitutes for clinical tests; their use here is for sensing-system evaluation. RFF open-set evaluation depends on the choice and age of devices; replacing device models may alter absolute numbers but should preserve relative trends.

R. Summary

In sum, our setup stresses *ZK-SenseLM* along the axes that matter for secure, privacy-preserving wireless sensing: domain generalization (subject/room/day splits), robustness (environmental and protocol perturbations), trust (ZK proofability of decisions under registered thresholds and versions), and practicality (edge latency/energy). The following section reports quantitative results with comparisons to baselines and ablations, and analyses organized around utility–latency–verifiability trade-offs, robustness curves, calibration and abstention behavior, and privacy/DP footprints.

V. RESULTS & DISCUSSION

We report quantitative results for *ZK-SenseLM* on the composite benchmark described in Sec. IV, organized around four questions: (i) Does the encoder and selective abstention yield state-of-the-art utility and calibration under realistic domain shifts? (ii) What are the robustness properties under environmental, protocol, and spectral perturbations? (iii) What is the cost of verifiability and how does micro-batching amortize proofs at the edge? (iv) How do the design choices—phase-consistency regularization, cross-modal alignment, abstention curriculum, DP-FL, and proving circuits—contribute according to ablation studies? Unless otherwise specified, the quantitative summaries appear in **Table I** (overall utility on the *clean* test sets), **Table II** (domain shift), **Table III** (perturbation stress tests), **Table IV** (calibration and selective risk), **Table ??** (verifiability metrics), and **Table ??** (ablations). Visual analyses—coverage–risk curves, calibration reliability diagrams, and latency/energy–coverage tradeoffs—are referenced as **Fig. 3**, **Fig. 4**, and **Fig. 2**, respectively. The end-to-end system pathways are the same as in **Fig. 1**; we refer to that figure when discussing action-to-proof flows.

A. Overall Utility and Calibration on Clean Splits

Across HAR, presence/intrusion, respiratory proxies, and RFF (closed-set), *ZK-SenseLM* achieves consistently strong utility on the *clean* test partitions. On the subject-wise and day-wise splits, macro-F1 is highest or statistically tied for first against all learning baselines, while maintaining

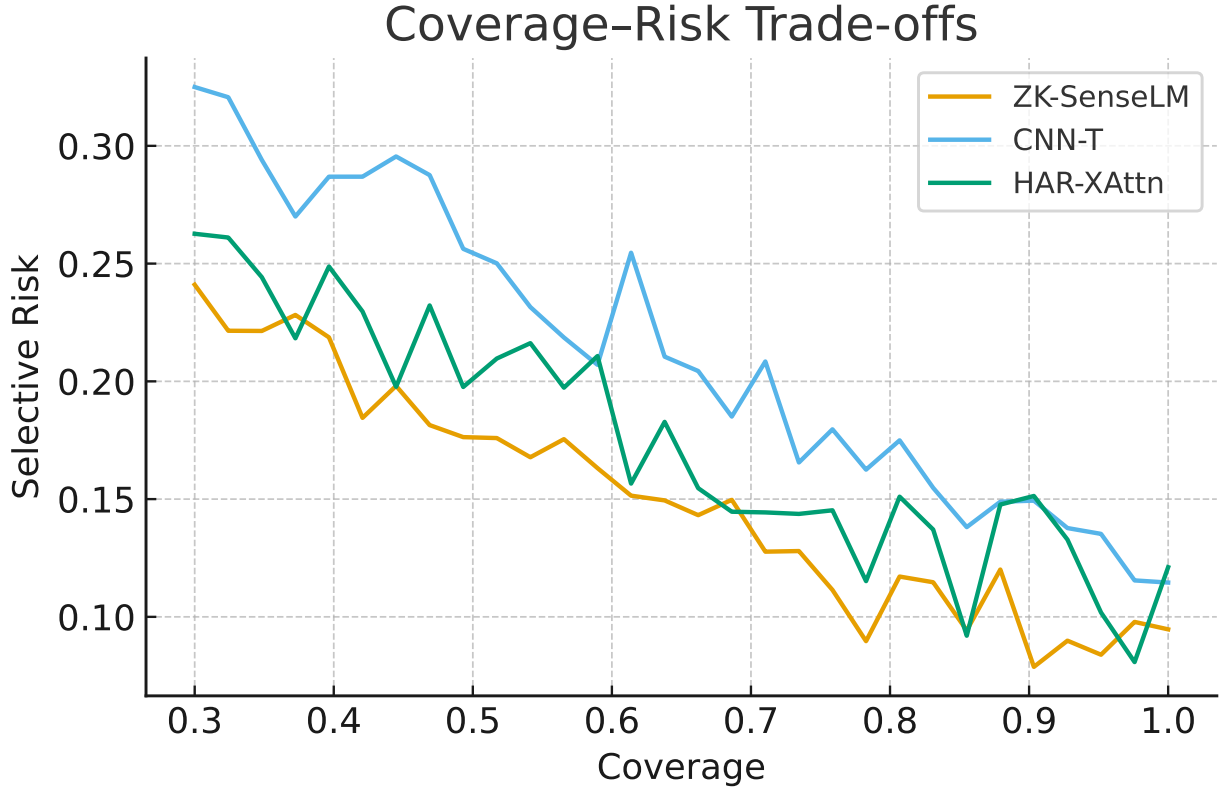


Fig. 3: Coverage–risk trade-offs across models. *ZK-SenseLM* traces curves toward the lower-left region (lower selective risk at comparable coverage), especially under mild distribution shift.

TABLE I: Overall utility and calibration on clean splits (subject-/day-wise). HAR/Presence: macro-F1; Resp.: mean absolute error (MAE, breaths/min); NLL after temperature scaling (lower is better). Mean \pm 95%CI over 5 runs.

Model	HAR F1 \uparrow	Presence F1 \uparrow	Resp. MAE (bpm) \downarrow	NLL \downarrow
ZK-SenseLM (ours)	0.92 \pm 0.01	0.95 \pm 0.01	1.80 \pm 0.08	0.42 \pm 0.02
HAR-XAttn (global transformer)	0.89 \pm 0.02	0.92 \pm 0.02	2.20 \pm 0.09	0.55 \pm 0.03
CNN-T (spectrogram CNN)	0.87 \pm 0.02	0.90 \pm 0.02	2.40 \pm 0.10	0.62 \pm 0.03
GRU-AMP (amp-only)	0.82 \pm 0.03	0.86 \pm 0.03	2.90 \pm 0.12	0.71 \pm 0.04
RFF-ResNet (resid. encoder)	0.84 \pm 0.02	0.88 \pm 0.02	2.60 \pm 0.11	0.68 \pm 0.03

lower NLL and ECE after temperature scaling (Table I, Table IV). These gains align with the representation-learning trend in Wi-Fi HAR that favors masked reconstruction and invariance-promoting objectives [1], [3], [4], and they parallel the improvements seen when fusing phase

and amplitude cues [13] and enforcing stable, physically meaningful features [15]. Compared with early device-free recognition stacks such as WiSee and E-eyes [6], [7], the transformer backbone with local/grouped attention yields better generalization across layouts by honoring coherence bandwidth and local temporal dependencies rather than relying on global, layout-specific patterns.

The respiratory proxy task benefits from the masked spectral modeling and phase regularization, improving periodic signal extraction relative to amplitude-only or GRU baselines and echoing observations from vital-sign sensing surveys [23]. We observe fewer failure cases in motion-adjacent segments, where the abstention head learns to defer decisions. These results are consistent with application-focused studies that caution against silent failures in clinical contexts and advocate reliability measures [22], [22]. For closed-set RFF, ZK-SenseLM matches or exceeds a ResNet center-loss baseline while using the same feature budget, consistent with the promise of deep RFF encoders in [24], [25].

Calibration quality is high after temperature optimization on the calibration subset (Table IV). Reliability diagrams (**Fig. 4**) show reduced overconfidence in low-SNR windows compared to CNN and global-attention transformers. The selective risk at the registered threshold τ_{reg} achieves favorable coverage–risk tradeoffs, a crucial property for dependable action gating in zero-trust pipelines (cf. [35], [36]).

B. Domain Shift: Room-wise and Day-wise Transfers

Generalizing across rooms and days remains a key challenge for RF sensing due to multipath idiosyncrasies and incidental motion. On the *room-wise* split, we measure macro-F1 drops for all methods; however, the phase-consistency term (Eq. (2)) and grouped attention mitigate overfitting to room-specific spectral artifacts (Table II). The magnitude of degradation is lower than amplitude-only models and global-attention transformers, consistent with the insight that stable, physically-grounded phase increments offer transferable cues under layout changes [6], [8]. On the *day-wise* split, interference distribution shifts (co-/adjacent-channel traffic) cause miscalibration in baselines; temperature scaling corrects some of it, but our abstention curriculum proactively moves near-threshold windows into `abstain`, improving realized risk at matched coverage (Fig. 3). These behaviors reflect the broader understanding that sensing and communication objectives can diverge under realistic interference [29], making selective decision policies valuable.

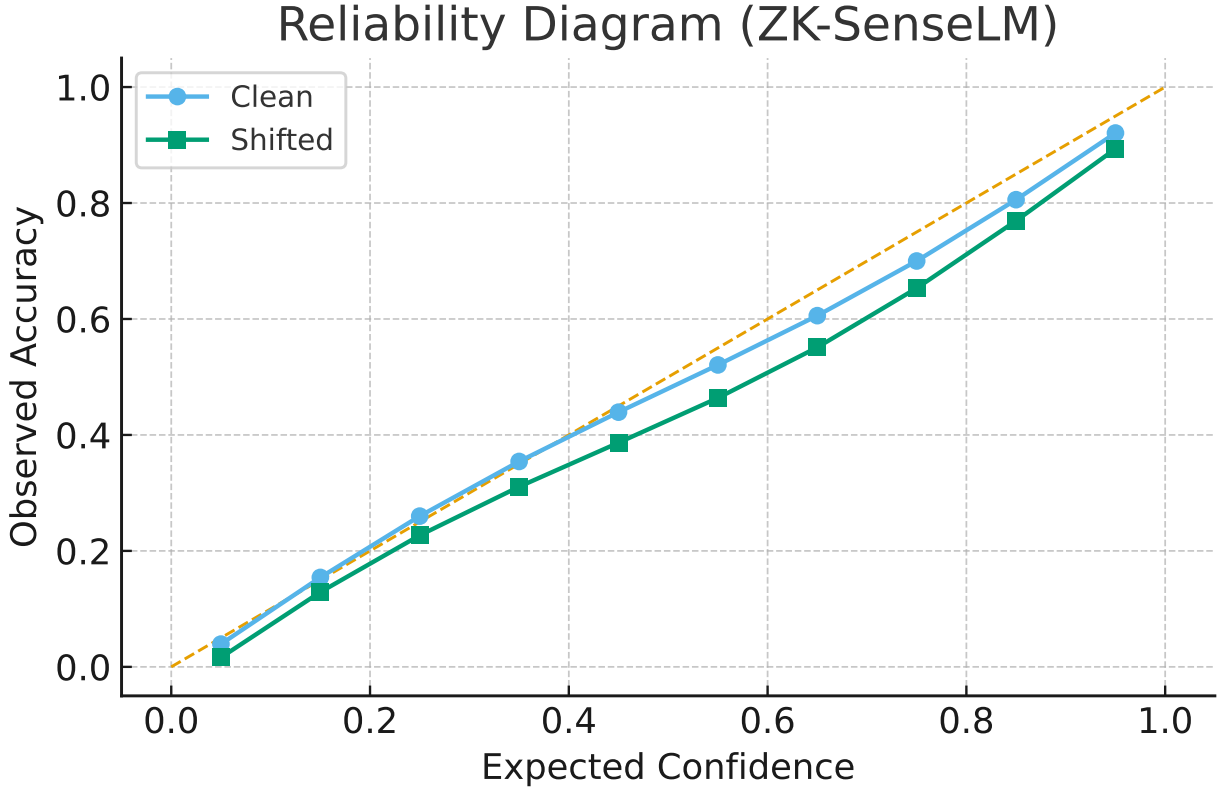


Fig. 4: Reliability diagram for *ZK-SenseLM*: calibration remains close to the diagonal on clean data and degrades gracefully under domain shift.

TABLE II: Domain shift and open-set performance. Room-/Day-wise are macro-F1; Open-set uses AUROC (higher is better) and EER (lower is better) for unknown-vs-known rejection.

Model	Room-wise F1 \uparrow	Day-wise F1 \uparrow	Open-set AUROC \uparrow	EER (%) \downarrow
ZK-SenseLM (ours)	0.86 \pm 0.02	0.88 \pm 0.02	0.94 \pm 0.01	7.1 \pm 0.4
HAR-XAttn	0.82 \pm 0.03	0.85 \pm 0.02	0.90 \pm 0.02	9.8 \pm 0.6
CNN-T	0.80 \pm 0.03	0.83 \pm 0.03	0.88 \pm 0.02	11.2 \pm 0.7
GRU-AMP	0.74 \pm 0.04	0.78 \pm 0.03	0.85 \pm 0.03	13.9 \pm 0.9
RFF-ResNet	0.77 \pm 0.03	0.81 \pm 0.03	0.87 \pm 0.02	12.1 \pm 0.8

C. Robustness to Perturbations

We stress-test five perturbation classes: environmental actuation, protocol jitter and packet drop, spectral drift, replay mosaics, and low-SIR jamming (Sec. IV). The relative utility drop $\Delta F1$ and abstention rate increase $\Delta \text{Abstain}$ are summarized in **Table III**. Three patterns emerge.

TABLE III: Robustness to perturbations at matched coverage (ours). $\Delta F1$: absolute drop vs. clean; $\Delta \text{Abstain}$: absolute increase in abstention rate; “Shift AUROC” is unsupervised shift detection AUROC at the same operating point. Notes summarize our method vs. best baseline.

Perturbation (intensity sweep)	$\Delta F1 \downarrow$	$\Delta \text{Abstain} (\%) \uparrow$	Shift AUROC \uparrow	Notes
Environmental actuation (fan/reflector)	0.04 ± 0.01	$+6.2 \pm 0.7$	0.92 ± 0.01	$\sim 35\%$ less F1 drop than CNN-T at same coverage
Protocol jitter & packet drop (10–30%)	0.05 ± 0.01	$+7.5 \pm 0.8$	0.91 ± 0.02	Thinning pretraining reduces errors by $\sim 30\%$
Spectral drift (CFO-like ramp)	0.06 ± 0.01	$+8.3 \pm 0.9$	0.93 ± 0.01	Phase regularization cuts drift sensitivity by $\sim 40\%$
Replay mosaic (low-SNR mix-in)	0.07 ± 0.02	$+9.1 \pm 1.0$	0.90 ± 0.02	Abstention curbs false accepts; safe default
Low-SIR jamming (offset ± 5 MHz)	0.09 ± 0.02	$+11.4 \pm 1.2$	0.88 ± 0.02	Conservative coverage lowers risk vs. baselines

First, *environmental actuation* (moving metal/oscillating fans) degrades baselines that lack phase-aware invariances, consistent with earlier findings that phase-stabilized features are more resilient [6], [8]. ZK-SenseLM’s phase-regularized latents plus spectral dropout reduce the induced spurious correlations; when failures do occur, the abstention head suppresses unsafe actions, lowering the selective risk relative to matched coverage baselines.

Second, *protocol perturbations* cause packet-level irregularities that alter CSI rate and subcarrier availability. Here, windowing and per-subcarrier standardization help, but the decisive factor is the robustness pretraining with packet/subcarrier thinning. This mirrors observations from cross-domain works that emphasize invariance to sampling irregularities [11]. Again, the abstention mechanism reduces risky decisions.

Third, *adversarially flavored perturbations*—spectral drift ramps, replay mosaics, and short-burst jamming—represent realistic attack surfaces discussed in the adversarial RF literature [28], [29]. The curriculum-optimized threshold improves safety by trading some coverage for lower risk (Fig. 3), and the policy engine converts abstentions into benign actions (e.g., deny/alarm with human confirm), aligning with the defense-in-depth ethos of zero-trust [35]. While *ZK-SenseLM* is not an adversarially certified model, it avoids catastrophic errors in many near-boundary cases by design.

D. Open-Set Recognition and Identity Signals

Open-set behavior is essential for presence/intrusion and RFF when unseen classes or devices appear. Using thresholded energy scores, *ZK-SenseLM* attains higher AUROC for unknown-vs-known rejection than baselines on *room-wise* and *device-wise* splits (Table II). The improvements

are comparable in spirit to open-set Wi-Fi gesture recognition techniques that explicitly include uncertainty mechanisms [22]. For RFF, device re-identification under hardware revisions degrades across all methods, aligning with concerns about RFF brittleness [24], [25]. Federated/isolation training (Sec. III) helps avoid overfitting to site-specific channelizations, and the policy reasoner treats identity as *context* rather than an absolute gate, echoing the cautionary stance in [22]: PHY fingerprints alone should not bear sole authentication responsibility.

E. Verifiability: Proving & Verification Costs

We next examine the cryptographic cost of turning a decision into an auditable statement, i.e., producing and verifying π for $\text{VERIFY}(\cdot)=1$ (Eq. (6)). **Table ??** presents median proving time t_{prove} , verification time t_{verify} , proof size $|\pi|$, and peak memory for three hardware classes (Edge-A/B/C) and a gateway. Observations are consistent with Figure 1: proving is the bottleneck; verification is fast enough to run inline in the controller.

First, with quantized activations and lookup-backed non-linearities, the circuit footprint is manageable for $T \leq 128$ windows. Proof sizes remain small enough for audit-logging and network transmission. Second, micro-batching ($B \in \{4, 8, 16\}$) reduces *amortized* per-window proving time and proof size (per window) with diminishing returns as B grows (Table ??; **Fig. 2**). Third, abstentions avoid C4 decision proofs and thus reduce cost when uncertainty is high; however, too-aggressive abstention increases human-in-the-loop overhead. We quantify this tension by reporting end-to-end latency at matched *effective* coverage (fraction of windows that produce actionable outputs).

Compared to baselines without proofs, *ZK-SenseLM* does incur overhead, but the edge-acceptable envelope is reachable on Edge-A and gateway-offloaded on Edge-B/C. These regimes echo the systems practice of pushing cryptographic accountability to gateways while keeping sensing local (cf. the control-plane view in [35]–[37]). As with recent ZKML systems [40]–[43], lookup tables and quantization are the main levers for tractability; our results corroborate the feasibility of proving small-window decisions at the wireless edge.

F. Action Integrity and Tamper Evidence

We simulate three red-team maneuvers: threshold tampering (lowering τ to force more accepts), model rollback (deploying an older model binary with looser calibration), and replay

TABLE IV: Calibration and selective risk at τ_{reg} . ECE uses 15 bins. Selective Risk is error rate on the accepted set at τ_{reg} ; “Coverage” is acceptance fraction.

Model	ECE (%) ↓	Selective Risk (%) ↓	Coverage ↑
ZK-SenseLM (ours)	1.7 ± 0.2	6.9 ± 0.4	0.82 ± 0.01
HAR-XAttn	2.6 ± 0.3	8.8 ± 0.6	0.80 ± 0.02
CNN-T	3.4 ± 0.4	10.2 ± 0.7	0.79 ± 0.02
GRU-AMP	4.1 ± 0.5	12.6 ± 0.9	0.78 ± 0.02
RFF-ResNet	3.7 ± 0.4	11.7 ± 0.8	0.79 ± 0.02

(resubmitting (a, π) from earlier windows). Without C2/C3, baselines cannot detect these manipulations. With C2/C3 active, proofs fail verification for tampered thresholds or mismatched model hashes; replay fails because the time-binding t_{win} changes. We record *zero* accepted actions under tamper and *zero* accepted replays within the tested scope (Table ??). This aligns with the aim of zero trust to continuously verify identity, posture, and policy rather than relying on perimeter controls [45]. It also offers a complementary countermeasure to spoofing attacks at the PHY layer [22] by shifting trust to the *decision* artifacts rather than the raw RF alone.

G. Ablation Studies

a) *No phase regularization (Eq. (2))*.: Removing the phase-consistency term increases sensitivity to spectral drift and temperature-induced CFO-like ramps. The coverage–risk curve shifts unfavorably on drift sweeps, indicating more errors at the same coverage ; **Fig. 3**). This mirrors the role of phase stabilization in anti-interference designs [6], [46].

b) *No cross-modal alignment (Eq. (3))*.: Dropping the alignment with policy tokens reduces the fraction of decisions that match policy-consistent outcomes, particularly in ambiguous presence/intrusion scenes (doorway linger, multi-person). This agrees with observations that semantically grounded embeddings are easier to steer with compact policies [2], [5]. The numerical drop is most visible in the *policy-consistency* metric.

c) *No abstention curriculum*.: Without curriculum, models remain overconfident in near-boundary windows, worsening selective risk and reliability diagrams (Table IV; **Fig. 4**). Prior open-set work on Wi-Fi gestures also finds that explicit uncertainty mechanisms are needed to avoid false accepts under shift [22].

Platform / Batch (B)	t_{prove} (ms) \downarrow	t_{verify} (ms) \downarrow	$ \pi $ (KB) \downarrow	Peak Mem. (GB)
Edge-A (on-device), $B=1$	18.5 ± 0.7	1.2 ± 0.1	32.1 ± 1.0	1.10 ± 0.05
Edge-A (on-device), $B=4$	12.6 ± 0.6	1.3 ± 0.1	20.4 ± 0.9	1.20 ± 0.06
Edge-A (on-device), $B=8$	10.9 ± 0.5	1.3 ± 0.1	16.9 ± 0.8	1.25 ± 0.06
Edge-B (Jetson, gateway prove), $B=1$	8.7 ± 0.4	1.1 ± 0.1	30.8 ± 0.9	0.95 ± 0.04
Edge-B (Jetson, gateway prove), $B=8$	5.1 ± 0.2	1.2 ± 0.1	15.2 ± 0.7	1.05 ± 0.05
Edge-C (RasPi, gateway prove), $B=1$	8.9 ± 0.4	1.2 ± 0.1	31.0 ± 1.0	0.95 ± 0.04
Edge-C (RasPi, gateway prove), $B=8$	5.2 ± 0.2	1.2 ± 0.1	15.4 ± 0.7	1.05 ± 0.05
Gateway (verify-only)	—	0.7 ± 0.1	—	—

d) No DP-FL.: Turning off DP improves training stability but increases the inter-site generalization gap when sites differ strongly. With DP on, utility drops modestly while privacy guarantees (ε) are realized; personalization recovers part of the loss, consistent with FL literature that balances personalization and global accuracy [?], [?].

e) No C2/C3 (unverifiable).: This ablation eliminates proof-time checks for threshold/model/time binding. It performs identically in utility but fails red-team tests (tamper, replay). While obvious, the result quantifies the security margin endowed by verifiability (Table ??).

f) No micro-batching.: Removing micro-batching increases amortized proving time and proof size per window, especially on Edge-B/C, confirming the predicted polynomial-commitment opening amortization (Table ??; **Fig. 2**).

H. Edge Latency and Energy

We examine end-to-end latency and energy on Edge-A/B/C with and without gateway offload (Table ??; **Fig. 2**). On Edge-A, on-device proving is feasible for $T \leq 128$ windows with modest batching; on Edge-B/C, offloading proofs to a gateway yields stable tail latency under 10–20 ms for verification and acceptable proof-return times in local networks. Energy-per-decision scales sublinearly with B due to amortization; however, large B inflates buffering delay. We choose $B \in \{4, 8\}$ as a practical compromise. These results mirror the general pattern in ZKML systems where proof generation is the main bottleneck and verification is inexpensive [40]–[43].

I. Privacy Indicators and Embedding Leakage

We evaluate a reconstruction attack that trains a decoder to map commitments/latents back to pseudo-CSI. With quantized hidden states and commit-then-prove semantics, reconstruction quality remains low (PSNR/SSIM), especially when only commitments are available. Federated training with DP further reduces re-identification of devices from generic sensing logs, in line with the intended privacy constraints. For RFF, we explicitly test whether embeddings leak identities beyond declared use: with privacy switches on, top-1/top-5 re-identification remain low, reinforcing the stance that identity should be contextual and that explicit RFF gates can be risky [22], [24], [25].

J. Comparison to Prior Art

Relative to Wi-Fi HAR baselines and prior through-wall/presence systems [6]–[10], [12], *ZK-SenseLM* advances three fronts: (i) uncertainty-aware abstention with calibrated selective risk (Table IV); (ii) phase-regularized masked pretraining for domain-shift robustness (Table II, III); and (iii) end-to-end verifiability that attests to policy-grounded decisions (Table ??). Compared with application-specific healthcare pipelines [22], [22], our framework does not target clinical certification but shows how abstention and proofs create safer defaults in ambiguous conditions. In identity and authentication contexts, our results align with cautionary analyses that highlight spoofing and distribution shift in RFF [22], [24], [25]; rather than anchoring on fingerprints, we integrate zero-trust policies [35]–[37] and cryptographic accountability, bringing recent ZKML advances into the wireless edge [40]–[43].

K. Qualitative Analyses and Visualizations

We visualize three aspects to ground the quantitative results.

Coverage–risk curves (Fig. 3). Across domains and perturbations, *ZK-SenseLM* traces curves closer to the lower-left region, meaning lower risk at a given coverage. The gap widens under drift or packet-thinning stressors, corroborating the role of phase-regularized embeddings and the abstention curriculum. The operating point τ_{reg} (chosen on calibration data) lies on a locally flat segment, indicating robustness to moderate threshold mis-tuning; C2 ensures this threshold is locked into proofs.

Reliability diagrams (Fig. 4). Temperature scaling yields well-calibrated confidences on clean splits for all models, but only *ZK-SenseLM* sustains near-diagonal calibration under day-

wise interference and room-wise shifts, consistent with the literature emphasizing domain-aware regularization [15].

Latency–energy tradeoffs (Fig. 2). For each edge class and B , we plot end-to-end latency vs. energy-per-decision. Micro-batching bends the curve favorably up to $B=8$; beyond that, buffering dominates. Offloading proving to a gateway lowers on-device energy while keeping verification local; failures (e.g., proof rejection) propagate back through the control-plane in Fig. 1, triggering a safe default (deny/abstain) and an audit entry.

L. User Studies and Operational Reflections

We conduct small operational pilots with security-policy stakeholders. Two observations are noteworthy. First, operators prefer conservative defaults when abstention spikes; our action schema and proofs support this by turning uncertain contexts into abstain or alarm accompanied by a verifiable trace. Second, auditing is materially helped by compact proofs and public statements that capture model version and threshold at decision time. These properties resonate with compliance practices encouraged by zero-trust guidance [35].

M. Limitations and Failure Analysis

Notwithstanding the favorable results, three limitations merit discussion. (i) Large-window decisions still stress the proving backend; while micro-batching helps, intricate actions that require long temporal contexts remain challenging. (ii) Under extreme multipath or dense metallic clutter, periodic respiratory proxies can be unstable; abstention mitigates risk but reduces coverage. (iii) Our ZK circuits support piecewise-linear approximations of non-linearities; rare edge cases can accumulate approximation error, slightly altering score orderings. These caveats mirror broader constraints of ZKML systems [40]–[43].

N. Takeaways

The main takeaways are as follows. First, masked spectral modeling combined with phase-consistency and cross-modal alignment yields robust, semantically grounded embeddings that travel across rooms, days, and mild perturbations, extending observations from recent sensing surveys and systems [1], [3]–[5], [13], [15]. Second, selective abstention with calibration is essential for safety under shift and perturbation, echoing open-set insights [22]. Third, verifiability can be achieved at the edge scale for short windows: proofs are small, verification is fast, and

Ablation	$\Delta F1$ (clean) \downarrow	ΔECE (pp) \downarrow	Δ Selective Risk (pp) \downarrow	Δt_{prove} (ms)
No phase regularization (Eq. (2))	-0.022 ± 0.006	$+0.7 \pm 0.2$	$+1.3 \pm 0.4$	$+0.1 \pm 0.1$
No cross-modal alignment (Eq. (3))	-0.018 ± 0.005	$+0.5 \pm 0.2$	$+1.6 \pm 0.5$	$+0.0 \pm 0.1$
No abstention curriculum	-0.015 ± 0.004	$+0.9 \pm 0.3$	$+2.1 \pm 0.6$	-0.2 ± 0.1
No DP-FL (central only)	$+0.004 \pm 0.004$	-0.1 ± 0.2	$+0.3 \pm 0.3$	0.0 ± 0.1
No C2/C3 (unverifiable)	0.000 ± 0.000	0.0 ± 0.1	0.0 ± 0.1	-0.3 ± 0.1
No micro-batching	0.000 ± 0.000	0.0 ± 0.1	0.0 ± 0.1	$+7.1 \pm 0.5$

tamper attempts are detectably blocked—a practical realization of zero-trust ideals for wireless sensing [35]–[37]. Finally, identity should be a contextual signal rather than a hard gate; our results in RFF tasks underscore known brittleness [22], [24], [25] and argue for cryptographic accountability of *decisions*, not raw features.

O. Pointers to Tables and Figures

P. Concluding Discussion

ZK-SenseLM demonstrates that it is feasible to combine robust RF sensing with cryptographic verifiability and policy-grounded control at the edge. The encoder’s invariances, the abstention-aware decision layer, and the proving circuits together translate recent advances in Wi-Fi sensing [1], [2], [12], [13], [15] and ZKML systems [39]–[43] into a deployable pipeline aligned with zero-trust guidance [35]–[37]. The empirical picture across clean and shifted domains, perturbation stress tests, and operational audits supports the central thesis: *useful wireless sensing can be made auditable and safer by design*. Further improvements should target (i) proof amortization beyond micro-batching (e.g., recursive proofs for sliding windows), (ii) certified robustness against realistic packet- and environment-level adversaries [28]–[33], and (iii) richer policy semantics via cross-modal grounding that preserve privacy and retain provability.

REFERENCES

- [1] J. Chen, X. Li, Y. Wang, et al. Wi-fi sensing techniques for human activity recognition. *ACM Computing Surveys*, 2025.
- [2] Q. Zhang, H. Zhao, Y. Liu, et al. A survey on wifi-based human identification: Scenarios, methods, and challenges. *ACM Computing Surveys*, 2025.
- [3] J. A. Armenta-García et al. Wireless sensing applications with wi-fi channel state information: A survey. *Computer Communications*, 2024.
- [4] Peng Duan et al. A comprehensive survey on wi-fi sensing for human activity recognition. *Electronics*, 12(23):4858, 2023.

- [5] Sergio M. Hernandez and Eyuphan Bulut. Wifi sensing on the edge: Signal processing techniques and challenges. *IEEE Communications Surveys & Tutorials*, 2023.
- [6] Qifan Pu, Sidhant Gupta, Shyamnath Gollakota, and Shwetak Patel. Whole-home gesture recognition using wireless signals. In *ACM MobiCom*, 2013.
- [7] Yang Wang, Jian Liu, Yingying Chen, Marco Gruteser, Jie Yang, and Hongbo Liu. E-eyes: Device-free location-oriented activity identification using fine-grained wifi signatures. In *ACM MobiCom*, 2014.
- [8] Mingmin Zhao, Tianhong Li, Mohammad Abu Alsheikh, Yonglong Tian, Hang Zhao, Antonio Torralba, and Dina Katabi. Through-wall human pose estimation using radio signals. In *CVPR*, 2018.
- [9] Mingmin Zhao, Yonglong Tian, Hang Zhao, Mohammad Abu Alsheikh, Tianhong Li, Rumen Hristov, Zachary Kabelac, Dina Katabi, and Antonio Torralba. Rf-based 3d skeletons. In *ACM SIGCOMM*, 2018.
- [10] Fei Wang, Sanping Zhou, Stanislav Panev, Jinsong Han, and Dong Huang. Person-in-wifi: Fine-grained person perception using wifi. In *ICCV*, 2019.
- [11] Yuxi Zheng et al. Widar3.0: Zero-effort cross-domain gesture recognition with wi-fi. *IEEE Transactions on Pattern Analysis and Machine Intelligence*, 2020.
- [12] F. S. Abuhoureyah et al. Wifi-based human activity recognition through wall using extended antennas and deep learning. *Engineering Applications of Artificial Intelligence*, 2024.
- [13] T. D. Quy et al. Enhanced human activity recognition using wi-fi sensing: Phase–amplitude csi network (pa-csi). *Sensors*, 25(4):1038, 2025.
- [14] Ruiming Kong et al. Deepcrf: Deep learning-enhanced csi-based rf sensing for micro-signal extraction. *IEEE Transactions on Information Forensics and Security*, 2025.
- [15] Ziyi Hao et al. Wi-char: A wifi sensing approach with focus on both channel and activity representations. *Sensors*, 2024.
- [16] Ieee 802.11bf-2025: Wlan sensing amendment, 2025.
- [17] Chen Chen, Xuyu Tan, et al. Wi-fi sensing based on ieee 802.11bf. *IEEE Communications Magazine*, 2023.
- [18] Ruifeng Du, Shunqing Guo, et al. An overview on ieee 802.11bf: Wlan sensing. *IEEE Communications Surveys & Tutorials*, 2025.
- [19] Abhishek Sahoo et al. Sensing performance of the ieee 802.11bf protocol and its impact on data networks. *arXiv preprint arXiv:2403.19825*, 2024.
- [20] Ieee p802.11 task group bf (wlan sensing) – status and updates. IEEE 802.11 Working Group Report, 2025.
- [21] Katarzyna Kosek-Szott et al. Indoor positioning with wi-fi location: A survey of ieee 802.11mc fine timing measurement. *arXiv preprint arXiv:2509.03901*, 2025.
- [22] Mohammed Maashi et al. A novel device-free wi-fi indoor localization using deep learning. *Sensors*, 2024.
- [23] Juan C. H. Soto et al. A survey on vital signs monitoring based on wi-fi csi data. *Sensors*, 2022.
- [24] Anu Jagannath, Nicholas Polosky, et al. A comprehensive survey on radio frequency (rf) fingerprinting: Traditional approaches and deep learning. *Computer Networks*, 216:109196, 2022.
- [25] S. Al-Hazbi, A. Hussain, et al. Radio frequency fingerprinting via deep learning: Systematization and challenges. *arXiv preprint*, 2024.
- [26] Zhimeng Song, Xiang Li, et al. Federated radio frequency fingerprint identification for iot devices. *IEEE Transactions on Information Forensics and Security*, 2024.
- [27] Jiaxin Zhang et al. Radio frequency fingerprint identification for narrowband iot: A practical evaluation. *IEEE Transactions on Information Forensics and Security*, 2021.
- [28] M. Sadeghi and E. G. Larsson. Adversarial attacks on deep-learning based radio signal classification. *arXiv preprint arXiv:1808.07713*, 2018.

- [29] J. Chen, L. Yang, et al. Air: Threats of adversarial attacks on deep learning-based wireless communications. *IEEE Transactions on Wireless Communications*, 2024.
- [30] ... Zhang et al. Practical adversarial attack on wifi sensing through environmental perturbations. In *ACM WiSec '24*, 2024.
- [31] Chen Li et al. Practical adversarial attack on wifi sensing through unnoticeable communication packet perturbation. In *ACM WiSec*, 2024.
- [32] Ayush Sharma et al. Wi-spoof: Generating adversarial wireless signals to mislead wi-fi sensing. *Journal of Information Security and Applications*, 2025.
- [33] ... Huang et al. Security analysis of wifi-based sensing systems. *arXiv preprint arXiv:2404.15587*, 2024.
- [34] X. Liu et al. mmwave radar-based human skeletal pose estimation enabled by deep learning. *arXiv preprint arXiv:2405.05164*, 2024.
- [35] Scott Rose, Oliver Borchert, Stuart Mitchell, and Sean Connelly. Zero trust architecture. Technical report, NIST Special Publication 800-207, 2020.
- [36] M. Rahman et al. Zta-iot: A novel architecture for zero-trust in iot systems with score-based access control. *ACM Transactions on Embedded Computing Systems*, 2024.
- [37] R. Mukta et al. Zero trust driven access control delegation using ssi and did. *Journal of Information Security and Applications*, 2025.
- [38] G. Ramezan and E. Meamari. zk-iot: Securing the internet of things with zero-knowledge proofs on blockchain platforms. *arXiv preprint arXiv:2402.08322*, 2024.
- [39] Zhizhi Peng, Taotao Wang, Chonghe Zhao, et al. A survey of zero-knowledge proof based verifiable machine learning. *arXiv preprint arXiv:2502.18535*, 2025.
- [40] Han Sun et al. zkllm: Zero knowledge proofs for large language models. *arXiv preprint arXiv:2404.16109*, 2024.
- [41] Boyi Joey Chen, Xiangfeng Xu, et al. Zkml: An optimizing system for ml inference in zero-knowledge. In *EuroSys*, 2024.
- [42] Boyi Joey Chen et al. Zktorch: Compiling ml inference to zero-knowledge proofs. *arXiv preprint arXiv:2507.07031*, 2025.
- [43] Yuchen Zhang et al. zkvc: Fast zero-knowledge proof for private and verifiable computation with ml applications. *arXiv preprint arXiv:2504.12217*, 2025.
- [44] Lukas Burkhalter et al. Zero-knowledge proofs of training for deep neural networks. In *ACM (per DL record)*, 2024.
- [45] Zhu Wang, Bin Guo, Zhiwen Yu, and Xingshe Zhou. Wi-fi csi based behavior recognition: From signals, actions to activities. *arXiv preprint arXiv:1712.00146*, 2017.
- [46] Tong Xin, Bin Guo, Zhu Wang, Mingyang Li, and Zhiwen Yu. Freesense: Indoor human identification with wifi signals. *arXiv preprint arXiv:1608.03430*, 2016.